Calhoun
Institutional Archive of the Naval Postgraduate School

Calhoun: The NPS Institutional Archive

DSpace Repository

Theses and Dissertations | 1. Thesis and Dissertation Collection, all items

1986-12

Characteristics of mesoscale island barrier cloud phenomena observed in satellite and space shuttle imagery.

Markley, David R. Jr.

http://hdl.handle.net/10945/21707

This publication is a work of the U.S. Government as defined in Title 17, United States Code, Section 101. Copyright protection is not available for this work in the United States.

Downloaded from NPS Archive: Calhoun

http://www.nps.edu/library

Calhoun is the Naval Postgraduate School's public access digital repository for research materials and institutional publications created by the NPS community. Calhoun is named for Professor of Mathematics Guy K. Calhoun, NPS's first appointed -- and published -- scholarly author.

Dudley Knox Library / Naval Postgraduate School
411 Dyer Road / 1 University Circle
Monterey, California USA 93943

TERE Y, CALIFORNIA 93943-5002

NAVAL POSTGRADUATE SCHOOL
Monterey, California

THESIS

CHARACTERISTICS OF MESOSCALE ISLAND BARRIER CLOUD PHENOMENA OBSERVED IN SATELLITE AND SPACE SHUTTLE IMAGERY

by

David R. Markley, Jr.

December 1986

Thesis Advisor: C. H. Wash

Approved for public release; distribution is unlimited

T230813

SECURITY CLASSIFICATION OF THIS PAGE

REPORT DOCUMENTATION PAGE

1a REPORT SECURITY CLASSIFICATION UNCLASSIFIED	1b. RESTRICTIVE MARKINGS
2a SECURITY CLASSIFICATION AUTHORITY	3 DISTRIBUTION/AVAILABILITY OF REPORT Approved for public release; distribution is unlimited.
2b DECLASSIFICATION/DOWNGRADING SCHEDULE	
4 PERFORMING ORGANIZATION REPORT NUMBER(S)	5 MONITORING ORGANIZATION REPORT NUMBER(S)
6a. NAME OF PERFORMING ORGANIZATION Naval Postgraduate School 6b OFFICE SYMBOL (If applicable) 63	7a. NAME OF MONITORING ORGANIZATION Naval Postgraduate School
6c. ADDRESS (City, State, and ZIP Code) Monterey, California 93943-5000	7b. ADDRESS (City, State, and ZIP Code) Monterey, California 93943-5000
8a NAME OF FUNDING/SPONSORING ORGANIZATION 8b. OFFICE SYMBOL (If applicable)	9. PROCUREMENT INSTRUMENT IDENTIFICATION NUMBER
8c. ADDRESS (City, State, and ZIP Code)	10 SOURCE OF FUNDING NUMBERS PROGRAM ELEMENT NO / PROJECT NO / TASK NO / WORK UNIT ACCESSION NO

11 TITLE (Include Security Classification)
CHARACTERISTICS OF MESOSCALE ISLAND BARRIER CLOUD PHENOMENA OBSERVED IN SATELLITE AND SPACE SHUTTLE IMAGERY

12 PERSONAL AUTHOR(S)
Markley, David R., Jr.

13a TYPE OF REPORT	13b TIME COVERED	14 DATE OF REPORT (Year, Month, Day)	15 PAGE COUNT
Master's Thesis	FROM _____ TO _____	1986 December	61

16 SUPPLEMENTARY NOTATION

17 COSATI CODES			18 SUBJECT TERMS (Continue on reverse if necessary and identify by block number)
FIELD	GROUP	SUB-GROUP	
			Atmospheric wake phenomena, von Karman vortices, island barrier effects, DMSP imagery, space shuttle imagery

19 ABSTRACT (Continue on reverse if necessary and identify by block number)

Mesoscale island barrier effects occur in the lee of islands and are observed in satellite imagery and in photographs from manned spaceflight missions. These phenomena arise when, in the presence of a low-level inversion, the boundary layer flow is disturbed by a barrier. Five types of island barrier effects are examined: a) von Karman vortices, b) single plumes, c) transitions from vortices to plumes, d) calm sea streaks and e) ship wake-like cloud patterns.

Results from 23 cases indicate a strong relationship between inversion height and type of barrier effect phenomena. A low, strong inversion was found for von Karman vortices cases while a higher, weaker inversion was present in the transition and plume cases. An inversion above the barrier occurred with wake phenomena. Wind shear structure appears important in the development of the calm sea streaks and the ship wake patterns.

20 DISTRIBUTION/AVAILABILITY OF ABSTRACT	21 ABSTRACT SECURITY CLASSIFICATION
☑ UNCLASSIFIED/UNLIMITED ☐ SAME AS RPT ☐ DTIC USERS	UNCLASSIFIED
22a NAME OF RESPONSIBLE INDIVIDUAL C. H. Wash	22b TELEPHONE (Include Area Code) 646-2295 / 22c OFFICE SYMBOL 63Wx

DD FORM 1473, 84 MAR 83 APR edition may be used until exhausted
All other editions are obsolete

SECURITY CLASSIFICATION OF THIS PAGE

Approved for public release; distribution is unlimited.

Characteristics of Mesoscale Island Barrier Cloud Phenomena Observed in Satellite and Space Shuttle Imagery

by

David R. Markley, Jr.
Lieutenant Commander, United States Navy
B.S., Muskingum College, 1974

Submitted in partial fulfillment of the
requirements for the degree of

MASTER OF SCIENCE IN METEOROLOGY AND OCEANOGRAPHY

from the

NAVAL POSTGRADUATE SCHOOL
December 1986

ABSTRACT

Mesoscale island barrier effects occur in the lee of islands and are observed in satellite imagery and in photographs from manned spaceflight missions. These phenomena arise when, in the presence of a low-level inversion, the boundary layer flow is disturbed by a barrier. Five types of island barrier effects are examined: a) von Karman vortices, b) single plumes, c) transitions from vortices to plumes, d) calm sea streaks and e) ship wake-like cloud patterns.

Results from 23 cases indicate a strong relationship between inversion height and type of barrier effect phenomena. A low, strong inversion was found for von Karman vortices cases while a higher, weaker inversion was present in the transition and plume cases. An inversion above the barrier occurred with wake phenomena. Wind shear structure appears important in the development of the calm sea streaks and the ship wake patterns.

TABLE OF CONTENTS

I. INTRODUCTION 9
A. HISTORY 9
B. MOTIVATION OF STUDY 10

II. BACKGROUND 12
A. TYPES OF BARRIER EFFECTS 12
B. DESCRIPTION OF ISLAND BARRIER EFFECTS TYPES 12
1. Von Karman Vortices 12
2. Single Cloud Plume 15
3. Transition from von Karman vortices to plumes 15
4. Calm Sea Streaks 16
5. Ship Wake 16
C. CLASSIFICATION OF BARRIER EFFECTS 17

III. DATA 19
A. CASES 19
B. SYNOPTIC DATA 19
1. Upper Air Soundings 19
2. Surface and Ship Observations 20
3. Surface and 850 mb Analysis Charts 20
C. SYNOPTIC VARIABLES 20
1. Inversion Strength 21
2. Inversion Height 21
3. Inversion Thickness 21
4. Surface Winds 21
5. Relative Humidity 22
6. Island Dimensions 22
7. Above Inversion Winds 22
8. Below Layer Stability 22

9. Above Layer Stability 23

IV. RESULTS AND CONCLUSIONS 24

A. RESULTS 24

1. von Karman Vortices 24

2. Single Plumes 26

3. Transitions from von Karman Vortices to Plumes 27

4. Calm Sea Streaks 27

5. Ship Wakes 29

6. Other Results 29

B. CONCLUSIONS 30

V. RECOMMENDATIONS 32

APPENDIX : TABLES AND FIGURES 34

LIST OF REFERENCES 57

INITIAL DISTRIBUTION LIST 59

LIST OF TABLES

1. SUMMARY OF VORTEX STREET PARAMETER VALUES 34
2. LIST OF CASES 35
3. BARRIER ISLAND DIMENSIONS 36
4. SYNOPTIC VARIABLE RESULTS SUMMARY 37
5. REYNOLDS NUMBERS CALCULATED FOR GUADALUPE ISLAND CASES 39

LIST OF FIGURES

1.1 Skylab photograph showing von Karman vortices in lee of Guadalupe Island off the coast of Baja California (SL3-122-2497) 40

2.1 Schematic diagram of (a) von Karman vortices leeward of an isolated island and (b) vortex street dimensional variables. After Chopra and Hubert (1975) 41

2.2 Single cloud plume in lee of Sirri Island, Iran taken from space shuttle mission STS-6 (S-6-45-068) 42

2.3 1920 GMT DMSP satellite image of 8 May 1973 showing von Karman vortices from Socorro Island and a single cloud plume from San Benedicto Island 43

2.4 2018 GMT DMSP satellite image of 15 June 1973 showing transition from von Karman vortices to single plume 44

2.5 Schematic diagram of the theoretical ship wake. Heavy lines denote wave crests. (After Hogner, 1922) 45

2.6 Skylab photograph showing ship wake clouds in lee of Antipodes Islands (SL4-137-3608) 46

2.7 Calm sea streaks in lee of Guadeloupe Island (Lesser Antilles) taken from space shuttle mission 41B (41B-32-1308) 47

4.1 Upper-air temperature profiles for cases showing von Karman vortices. Profiles have been shifted to a common surface temperature of 17 °C 48

4.2 Same as Fig. 4.1 but for cases showing single plumes 49

4.3 Same as Fig. 4.1 but for cases showing transition from von Karman vortices to single plumes 50

4.4 Temperature and dew point profiles for calm sea streak cases showing profiles similar to von Karman vortices. Note $T\text{-}T_d$ separation below inversion layer 51

4.5 Temperature and dew point profile for von Karman vortices case S-8. Dew point depression shows higher moisture in boundary layer as compared to Fig 4.4 52

4.6 Comparison between calm sea streak case F-9, with plume profile and plume case, S-5. Note difference in moisture in boundary layer 53

4.7 Same as Fig. 4.1 but for cases showing tropical western ocean calm sea streaks 54

4.8 Station plots showing surface (solid) and upper air (dashed) winds. A. von Karman vortices, B. transition, C. plume, D. sea streak, E. ship wake and F. western ocean sea streak 55

4.9 Same as Fig. 4.1 but for cases showing ship wake pattern 56

ACKNOWLEDGEMENTS

The completion of this study was made possible by the generous assistance of many individuals. I would like to thank Dr. Robert Fett of the Naval Environmental Prediction Research Facilty (NEPRF) for the use of island barrier effects satellite imagery from his extensive collection and for his assistance in reviewing the thesis results. I am indebted to the NEPRF METLAB staff for their efforts in providing the synoptic dataset and to Mr. Mike McDermet for drawing many of the figures used in this thesis. I would like to thank Dr. Philip Durkee, my second reader, for his insightful questions which contributed to a better study. To my thesis advisor, Dr. C. H. Wash, I extend my deepest gratitude and appreciation for his efforts in providing the space shuttle photographs and for his continuing concern, guidance and support throughout the thesis process. Finally, I would like to publicly acknowledge the love and patience of my wife, Kathy, and my daughter, Meghan, without whose support this study would not have been possible.

I. INTRODUCTION

The extent and variety of barrier-induced mesoscale cloud phenomena was not appreciated until the advent of satellite imagery in the 1960's. Unlike thunderstorms or tornadoes, these phenomena were too large to be seen by individual ground or airborne observers. At the same time, these cloud phenomena were too small to be picked up by the synoptic-scale observation network, as would a frontal system or tropical storm. Some of these mesoscale cloud phenomena are the island barrier effects. These effects arise from the interaction of the low-level wind flow with the mountainous topography of many islands. The result is a disturbance in the flow which is revealed in the cloud patterns predominantly downstream of the island.

A. HISTORY

With the launch of the first Television Infrared Observation Satellite (TIROS-1) in 1960, meteorologists had an observation system with sufficient altitude to see island barrier effects. One of the earliest TIROS satellite studies of mesoscale cloud patterns (Bowley *et al.*, 1962) focused on wake clouds under low-level inversions. Hubert and Krueger (1962), using TIROS III imagery, were probably the first to report von Karman vortices as an island barrier effect. As an example of this barrier effect, Fig. 1.1 shows von Karman vortices in the lee of Guadalupe Island. With each new generation of improved weather satellites, additional island barrier effects were studied. Tsuchiya (1969) used images from the Environmental Science Services Administration (ESSA) 7 and 8 satellites to study the motion of von Karman vortices. Although not a weather satellite, the Landsat satellite program has collected imagery of mesoscale cloud phenomena, as reported by Ormsby (1977). Images from the National Oceanic and Atmospheric Administration (NOAA) 4 satellite appeared in Thomson *et al.* (1977), while Fett and Mitchell (1977) makes extensive use of Defense Meteorological Satellite Program (DMSP) and Geostationary Operational Environmental Satellite (GOES) satellite images. Work continues in the study of the island barrier effects using current DMSP, NOAA and GOES satellites.

While operational satellites provide imagery of the island barrier effects, large numbers of images must be examined to identify examples of these phenomena. Human observers, located in the right spot, can selectively record island barrier

phenomena which eliminates the problem of searching through considerable amounts of satellite imagery in order to find examples of barrier effects. The National Aeronautics and Space Administration (NASA) manned space program places human observers at lower orbits (150-300 km) than the unmanned environmental satellites (800 km). These observers can see meteorological phenomena developing and record the regions of interest with hand-held cameras. This ability to selectively record phenomena of interest provides high quality images without the need to examine large numbers of photographs. The hand-held cameras also offer higher resolution and clearer imagery of the cloud phenomena than do the operational satellite sensors. A discussion of the use of photographs from the Space Transportation System (STS), or Space Shuttle, is contained in Svetz (1985).

The use of photographs from manned spacecraft to study the island barrier effects parallels the operational satellite imagery studies. Hubert and Krueger (1962) included a photograph of von Karman vortices taken on the Project Mercury MA-4 flight. The crew of the Gemini 6 spacecraft photographed clouds near the Canary Islands which Zimmerman (1969) used in his study. In the Apollo era, extensive study of mesoscale cloud phenomena occurred using the photographs obtained by the Skylab missions (Fujita and Tescon (1977) and Pitts *et al.* (1977)). Black (1978) reported on the mesoscale cloud patterns observed and photographed during the Apollo-Soyuz mission. And more recently, the Space Shuttle program has extended the abilities of manned data collection through the use of mission specialists who have been trained in meteorological earth observation.

B. MOTIVATION OF STUDY

With the increasing availability of satellite imagery to at-sea meteorologists, knowledge of island barrier effects can contribute to operational use in assessing current meteorological conditions and in forecasting. By understanding the atmospheric conditions required for the formation of island barrier effects, the aircraft carrier or staff meteorologist can determine, from the existance of these phenomena, the current and past history of the wind flow patterns and the atmospheric stability for the region in the vicinity of the island producing the barrier effect.

As an example, consider a carrier battle group (CVBG) operating near the west coast of Africa. In this environment local meteorological observations are sparse and of questionable accuracy. With an image containing a von Karman vortex street from

a nearby island, such as the Canary Islands, and a proven barrier effects characterization scheme, the carrier meteorologist could estimate variables such as the low-level wind field, the height of the near surface inversion and the length of time these conditions had existed.

While there are numerous case studies of barrier effects, these studies generally emphasize and describe different factors of a single barrier effect. Although some authors provide collections of barrier effect examples, e.g. Fett and Mitchell (1977) and Fujita and Tescon (1977), presently no overview analysis exists which compares various types of barrier effects using consistent data for each type. This lack of an overview of the barrier effects provides motivation for this thesis.

The thesis objectives are:

1) Conduct analysis of many island barrier effects cases to determine the atmospheric structure associated with the phenomena.

2) Identify meteorological and physical parameters which characterize the various types of island barrier effects.

3) Develop a scheme for identifying atmospheric conditions in data sparse regions based on imagery and behavior of the characteristic parameters of island barrier effects.

II. BACKGROUND

A. TYPES OF BARRIER EFFECTS

The mesoscale island barrier effects separate into five types, based on their physical appearance as seen in satellite or shuttle imagery. These five types are:

1) von Karman vortices
2) single cloud plume
3) transition from von Karman vortices to single plume
4) calm sea streaks
5) ship wake

In this chapter, these five types of barrier effects will be described using observations and theories discussed in previous studies.

B. DESCRIPTION OF ISLAND BARRIER EFFECTS TYPES

1. Von Karman Vortices

Von Karman vortices, or vortex streets, are named for their resemblance to vortices produced in laboratory experiments of fluid flow around objects. Von Karman's (1911) theoretical formulation provides the basis for these laboratory-produced vortices. Later researchers adopted the terms "von Karman vortices" or "von Karman vortex street" to describe this phenomenon.

As described by Chopra (1973), the von Karman vortex street is composed of two parallel rows of vortices with a vortex from one row positioned midway between two adjacent vortices of the second row. The two rows of vortices are produced by a two dimensional fluid flow around a cylindrical object. The vortices of each row rotate in the same direction, but the two rows of vortices rotate in opposite directions. Figure 2.1 illustrates the pattern of von Karman vortices around an isolated island and shows the rotation of the individual vortices.

Atkinson (1981) discusses several parameters from laboratory analysis which describe two dimensional von Karman vortices produced in the lee of cylinders. These parameters include the spacing ratio (h/a), the Reynolds number (Re), the Strouhal number (St), the Lin parameter (β), the eddy viscosity (ν), the vortex propagation speed (u_c) and the period of vortex formation (T).

One parameter which can be obtained from satellite imagery, after the images have been rectified to remove the effects of earth's curvature and the obliqueness of sensor view angle, is the spacing ratio, h/a. This ratio of lateral street width (h) to longitudinal spacing (a) characterizes the vortex street geometry and has an empirical range of 0.28-0.50 (Chopra, 1973). The velocity ratio, u_c/u, is related directly to this spacing ratio. Thus, from measurements of h, a and u, the mean wind flow, the vortex propagation speed can be determined. The period of vortex formation, T, is the reciprocal of the vortices shedding frequency, N (or j as in Table 1). This frequency can be calculated from values of a and u_c using the equation,

$$N = u_c/a. \tag{2.1}$$

The values for u_c and N can also be derived if two images of a vortex street are available with a small temporal separation. Measurement of the translation of the vortices from one image to the next and knowledge of the time separation between the images permits calculation of u_c and hence, N, through Eqn. 2.1. The Lin parameter, β, is also related to the spacing and velocity ratios. So, with values for h, a and u the descriptive parameters discussed below can be determined.

The Reynolds number (Re) is the ratio of the mean wind flow speed (u) and barrier diameter (d) to the viscosity of the fluid (ν), or

$$Re = ud/\nu. \tag{2.2}$$

Laboratory calculations of Reynolds number values use the kinematic (molecular) viscosity in Eqn. 2.2. However, in order to obtain comparable Reynolds numbers for meteorological phenomena, such as von Karman vortex streets, the eddy viscosity must replace the kinematic viscosity in the equation. As discussed by Chopra (1973), this use of the eddy viscosity is required because the scales of the meteorological phenomena are much larger than those of the laboratory phenomena. Chopra states that the Reynolds numbers for laboratory produced von Karman vortices are in the range $40 < Re < 1000$. Atkinson (1981) gives the laboratory range as $40 < Re < 200$. Atkinson also summarizes data from prior studies of von Karman vortices produced by island barriers. This summary, included as Table 1, shows that Reynolds numbers of these studies generally lie within the 40-200 range.

The Strouhal number (St) is the ratio of the frequency of vortex shedding (N) times barrier diameter (d) to the mean fluid flow (u), written as

$$St = Nd/u. \tag{2.3}$$

For laboratory observed von Karman vortex streets, Chopra gives the range for the Strouhal number as $0.1 < St < 0.21$, while Atkinson gives this range as $0.12 < St < 0.19$. The observed values shown in Table 1 generally lie within these laboratory values.

The Reynolds and Strouhal numbers can be combined to obtain a third parameter which is independent of the diameter of the barrier to the fluid flow. This parameter, the Lin parameter (β), is the ratio of the Reynolds number to the Strouhal number. In this ratio, the barrier diameter terms cancel out, leaving

$$\beta = \nu N/u^2. \tag{2.4}$$

Lin (1959) found that the values of β for stable vortex streets behind cylinders range from 1.0×10^{-3} to 2.5×10^{-3}.

Chopra (1972) states that the Lin parameter best characterizes von Karman vortices because: a) these vortices occur behind objects of varying diameters and the Lin parameter is independent of diameter; b) the appropriate velocity field associated with the fluid flow gives rise to the vortices; and c) the range for β is more restricted than the range for the Reynolds and Strouhal numbers. Although the Lin parameter may be a better descriptor from a fluid dynamics point of view, it is not a practical measure for synoptic observation and forecasting. Calculations of the frequency of vortex shedding (N) require multiple satellite images of a von Karman vortex street taken at different times or a rectified image from which h and a can be measured. Unfortunately, most of the available imagery does not have the necessary temporal separation. There are also problems with measuring h and a on a rectified image. The appearance of the vortex street in an image depends on the amount of clouds present below the inversion, which creates difficulties in determining the exact spacing between vortices. Another factor limiting the usefulness of β is the variability of the eddy viscosity term. Heffter (1965) gives experimental values for the eddy viscosity which vary from 10 to 10^5 m^2s^{-1}. Most of the previous studies of the mesoscale von Karman vortices assume values for h/a and/or β in order to derive values for N and ν. With a

value for β and/or ν, the Reynolds number can be easily derived from available synoptic data (mean wind flow and island diameter) and provides a descriptive parameter for the von Karman vortices.

Most of the previous studies, such as Chopra (1973), characterize the meteorological conditions for formation of von Karman vortices as: a) a low-level inversion (altitude of 0.5 to 1.5 km); b) a steady wind flow over a period of several hours; and c) an orographic barrier, such as an island. The low-level inversion provides a cap over the island barrier which directs the wind flow around the barrier instead of allowing more normal wind flow over the island. This creates the essentially two-dimensional wind field in which the vortex streets develop.

2. **Single Cloud Plume**

The single cloud plume is related to the von Karman vortex street. Figure 2.2 displays an example of a plume in the lee of the Sirri Island, Iran. Previous studies suggest that single plume formation occurs when the wind field, island barrier diameter, or eddy viscosity is such that the Reynolds number is less than the value needed to produce a von Karman vortex street ($Re < 40$). Figure 2.3 shows von Karman vortices in the lee of Socorro Island and a single cloud plume from nearby San Benedicto Island. Fett and Mitchell (1977) state that the difference in the two barrier effects stems from the difference in size between the two islands. With similar wind fields, the larger diameter of Socorro generates von Karman vortices while the smaller San Benedicto has a smaller Reynolds number, resulting in a plume. Tsuchiya (1969) provides photographs of flow patterns for various Reynolds number values. These photographs show single plume patterns in the flow for Reynolds numbers less than 65. However, Chopra (1973) cautions against drawing conclusions concerning Reynolds numbers for observed vortex streets based on similarity with photographs of laboratory produced flow patterns. Although the Reynolds number is useful in describing the fluid dynamics of von Karman vortices, as will be shown in later chapters, this parameter is not a useful means of separating plume cases from those with von Karman vortices.

3. **Transition from von Karman vortices to plumes**

Imagery also provides cases where both von Karman vortices and single plumes are present in the flow downstream from the barrier island. One example image of this type is presented in Fig. 2.4. The development of both mesoscale barrier effects from one barrier suggests that changes in atmospheric structure and/or wind flow are causing a shift from one phenomenon to the other.

4. **Calm Sea Streaks**

Space shuttle photography and satellite imagery show the presence of long streaks on the ocean surface extending out from the lee of island barriers. Based on images showing sunglint patterns, such as Fig. 2.7, these streaks appear to be regions with a calmer sea surface than that of the surrounding area. Sunglint occurs when the direct rays of the sun are reflected by the ocean surface directly into the satellite sensor or spacecraft camera and appears in imagery as a bright or very light region. A region of calm seas has a higher reflectivity and appears as a bright area in the sunglint pattern, while rougher sea surface scatters the sunlight away from the sensor and appears as a dark area. In regions adjacent to the sunglint, the calm areas appear as dark patches in the image while rough sea areas appear as lighter areas. Although imagery exists which shows calm sea streaks as dark areas, no cases of this type were included in this study. Fett and Rabe (1975), using DMSP imagery and numerical modeling, find that calm seas occur in the lee of islands and can extend downstream up to 200-300 km.

Since the calm sea streaks appear in relatively cloud-free images, the question of relationship to other barrier effects arises. Chopra (1973) states that the complex ocean eddies found in the lee of the Hawaiian Islands originate from the energy transfer from the strong winds and atmospheric eddies (barrier effect eddies) to the ocean surface via air-sea interaction mechanisms. He believes that the energy transfer occurs before the barrier effect eddies move sufficiently downstream from the islands to form the cloud patterns associated with the barrier effects. Nickerson and Dias (1981) report the presence of vortex streets similar to von Karman vortices in the lee of Hawaii, but note that often insufficient moisture is present in these vortices to form the cloud shapes. Thus, the Hawaiian Islands provide one example where mesoscale barrier effects are revealed by oceanic instead of atmospheric phenomena. This supports the idea that calm sea streaks may be cloudless manifestations of island barrier effects.

5. **Ship Wake**

Fujita and Tescon (1977) believe that atmospheric wake clouds are similar in origin to the wakes produced by ships moving through the water. Kelvin's (1887) theory indicates that an object moving in a straight line through a fluid generates the V-shaped wake pattern. Figure 2.5 shows a schematic diagram of the theoretical ship wake based on the study by Hogner (1922). Two kinds of waves form in the wakes of

moving objects: a) divergent waves, which are the familiar V-shaped waves and b) transverse waves, which are waves connecting the sides of the divergent waves. Havelock (1950) shows that when the velocity (c) of the object is large compared to the depth of the fluid (h) the transverse waves disappear. The equation for this relationship is

$$c^2/gh > 1 \qquad (2.5)$$

where g is the acceleration due to gravity.

Fujita and Tescon (1977) state that wake theory seems applicable to the atmosphere. In the atmospheric application, the fluid (air) moves around a stationary object (e.g. an island barrier), instead of a moving object (ship) in a stationary fluid (water). One of these atmospheric ship wakes is shown in Fig. 2.6. Thus, based on wake theory, two situations arise for atmospheric wake waves: a) divergent and transverse waves within a deep layer of slow moving air below a capping inversion, and b) divergent waves within a more shallow layer having a higher velocity wind flow.

In their study of stratus cloud phenomena, Edinger and Wurtele (1972) described ship wake clouds, which occurred in the lee of San Nicolas Island, as a type of gravity waves. They state that when a fluid has its stability concentrated in an interface layer and flows over a limited obstacle, a gravity wave resembling a ship wake is formed. With the atmosphere as the fluid, an inversion as the stable interface layer and a barrier island as an obstacle to fluid flow, a ship wake shaped gravity wave pattern forms. Edinger and Wurtele did not observe transverse waves in San Nicolas Island ship wake patterns but do not rule out this type of wave structure in atmospheric wakes.

C. CLASSIFICATION OF BARRIER EFFECTS

Most of the prior studies of island barrier effects have concentrated on a single type, such as von Karman vortices, and have not attempted to link these mesoscale phenomena together. To produce useful tools for analysis and forecasting, a comprehensive classification scheme, using readily available synoptic meteorological parameters must be developed. Previous classification schemes are given below.

Fujita and Tescon (1977) divide the mesoscale cloud patterns into three types based on lapse rate, wind velocity and barrier size. These types are:

1. Cumulus streets - Form when the near-surface lapse rate is adiabatic (identifies unstable air) and a slow to medium wind velocity.

2. Von Karman vortex streets - Form when the near-surface lapse rate ranges from a small positive to a negative value (indicates stable air), the low-level wind velocity is slow to medium and the barrier is relatively large.

3. Ship wake clouds - Form when the near-surface lapse rate is a small positive value, the wind velocity is medium to fast and the barrier is relatively small. Above a critical wind velocity, the transverse waves cease.

The primary problem with this classification scheme is that the wind velocities and barrier sizes are not clearly specified. For von Karman vortices, the Reynolds number relates wind velocity to barrier size. A high wind velocity coupled with a small island barrier could produce the same Reynolds number, and hence von Karman vortices, as a large island with slow wind velocity.

Fett and Mitchell (1977) provide a series of case studies to illustrate the various barrier effects seen in satellite imagery. This series includes some twenty cases, but several cases are similar and no classification of the barrier effects according to synoptic parameters is made. However, Fett and Mitchell include more types of the barrier effects than do Fujita and Tescon (1977), and thus give a more complete description of these phenomena.

Having examined the previous studies of mesoscale island barrier effects and some proposed classification schemes, the following questions form the investigative basis for this thesis research.

1. What are the characteristic parameters common to the various island barrier effects?

2. Which of the characteristic parameters permits differentiation between and classification of the various barrier effects?

3. What is the relationship (if any) between the calm sea streaks and other barrier effects?

4. Can a simple and useful classification scheme, based on easily obtained synoptic data be developed?

5. Can this classification scheme be used as a forecast or nowcast aid?

III. DATA

A. CASES

Satellite imagery and manned spaceflight photographs containing mesoscale island barrier effects came from two sources. The Naval Environmental Prediction Research Facility (NEPRF)[1] provided DMSP images. One image from GOES was also included, giving a total of nineteen potential cases from satellite imagery. The Department of Meteorology at the Naval Postgraduate School[2] provided a second set of imagery from Skylab, Apollo-Soyuz and STS manned space missions. This set formed the basis for eleven potential cases. The combined number of potential imagery cases was thirty.

In addition to the imagery, an extensive synoptic data set was required to develop the necessary physical variables for closer examination and correlation. Because this requirement was so stringent, seven of the 30 potential cases had to be eliminated, leaving a total of 23 cases for this study. Table 2 lists these cases, providing the locations, dates and times of the images.

B. SYNOPTIC DATA

In addition to the barrier effect satellite images and NASA mission photographs, the supporting synoptic data were required. This data set was obtained from the Fleet Numerical Oceanography Center (FNOC) and consisted of upper-air soundings, surface and ship synoptic observations, and surface and 850 mb objective analysis fields from the Navy Operational Global Atmospheric Prediction System (NOGAPS). The data were used to evaluate a variety of synoptic variables as possible candidates for characterizing the various island barrier effects.

1. Upper Air Soundings

For each case, four upper-air soundings were collected. These four soundings were the 12 GMT sounding of the day prior to image time, the 00 GMT and 12 GMT soundings of the image date, and the 00 GMT sounding for the day after that of the image. These soundings were either taken from the barrier island or from the sounding station nearest the island. This scheme bracketed the image time (three soundings

---

[1]Dr. Robert W. Fett, NEPRF

[2]Dr. C.H. Wash, NPS

before and one after) and, since the mesoscale barrier effects have lifetimes on the order of 18 to 30 h, placed emphasis on the conditions existing prior to the image time. The soundings and associated data listings provided vertical profiles of temperature and dew-point temperature, along with tabulated values of temperature, dew-point temperature, pressure level, relative humidity and upper-air winds.

2. Surface and Ship Observations

Surface and ship observations were collected for a 6° latitude by 6° longitude region centered on the location of the barrier island. The data were generated at three hour intervals for the period covered by the soundings. i.e., 12 GMT from the day prior to the image day through 00 GMT on the day following that of the image. The surface observations occurring on the barrier island were used to define the surface wind flow whenever possible. In a few cases, no surface observing station was present; therefore, the observations reported by the nearest ship were used to derive the surface winds. Ship reports were also used to confirm that the island station observation of surface wind was representative of the wind flow beneath the capping inversion.

3. Surface and 850 mb Analysis Charts

Surface analysis charts covering a 30° latitude by 30° longitude region centered on the barrier island location were used. These charts, which encompassed the same 36 h period as the surface observations, provided the surface pressure fields which were used to verify that island observed surface winds were representative of the regional wind flow. Surface and ship observations were also plotted on these charts, permitting graphic description of ship and surface observations as well as location of the ship report with respect to the barrier island. NOGAPS 850 mb analysis charts were used to extract the 850 mb height and wind field for the region surrounding the barrier island. These charts, spanning the same time period and region as the surface analysis charts, provided the regional wind field above the inversion layer for most cases.

C. SYNOPTIC VARIABLES

In order to characterize the various island barrier effects, a variety of synoptic and physical variables were evaluated. These variables were based on the synoptic situations described in previous studies. Thus, variables were chosen which examined the inversion, wind flow, stability of the lower atmosphere and dimensions of the island. Descriptions of these variables and associated calculations are now discussed.

1. Inversion Strength

One of the key variables in characterizing the mesoscale island barrier effects is the inversion strength. This quantity is a measure of the strength of the capping inversion, or the rigidity of the lid which forces the two-dimensional flow around the island barrier. The inversion strength is the lapse rate of the inversion layer, defined as the change in temperature divided by the change in height, or $\Delta T/\Delta Z$. The units are the same as those of the lapse rate, °C/km.

2. Inversion Height

Given a capping inversion, the inversion height determines whether or not the wind flow goes over or around the island barrier and the appropriate cross sectional diameter of the barrier. Calculations of the inversion height used the hypsometric equation (Holton, 1979),

$$\Delta Z = RT/g \ln(P_2 / P_1). \qquad (3.2)$$

In this equation, ΔZ is the height difference in meters of the layer of interest (in this case the layer from the surface to the inversion base), R is the gas constant for dry air (287 J kg^{-1} $°K^{-1}$), T is the mean temperature of the layer in degrees Kelvin, g is the acceleration due to gravity (9.80665 m s^{-2}), and P_2 and P_1 are the top and bottom pressure levels of the layer, respectively, in millibars. In the calculation of the inversion height, the surface is assumed to occur at $Z_1 = 0$ m; therefore, ΔZ equals Z_2, the height of the inversion base.

3. Inversion Thickness

The inversion thickness is the thickness, ΔZ, of the inversion layer and is measured in meters. Values for this variable were calculated using Eqn. 3.2, where P_2 and P_1 are the pressure levels at the top and bottom (base) of the inversion layer, respectively.

4. Surface Winds

As stated above, the mean regional wind flow beneath the capping inversion is represented by the surface winds. This mean flow is that flow which occurs upstream of the barrier island prior to the mesoscale interactions and the wind flow occurring to the sides of the mesoscale barrier effects phenomenon. The data used in the evaluation were from the surface observation closest in time to that of the image. These surface observations were compared to any available ship observations near the barrier island

and with the regional wind flow, determined from the isobars of the surface analysis charts. These comparisons showed that barrier island surface observations did represent the mean wind flow.

5. Relative Humidity

Relative humidity values were taken directly from the sounding data. The values used were the maximum values either at, or just below, the level of the inversion base. This variable was examined to determine, between the various case types, if any significant differences existed in the moisture content in the atmosphere below the inversion.

6. Island Dimensions

Since the barrier island must penetrate the inversion to reduce or eliminate the wind flow over the island and since the diameter or width of the barrier plays a role in determining the Reynolds number, the dimensions of the barrier island are also important. These dimensions included the height of the highest elevation of the island in meters and the diameter (or width) of the barrier to the wind flow in kilometers. The heights and diameters for the barrier islands used in this study are given in Table 3. Since the island of Guadalupe dominated the cases, its diameter values were measured at elevations corresponding to average inversion heights (500 and 1000 m) and to the predominant wind directions occuring in the data set.

7. Above Inversion Winds

In order to determine any contribution to the formation of mesoscale island barrier effects by the wind flow above the inversion layer or by the wind shear across the inversion, the winds above the inversion were examined. Because of the relatively constant nature of wind flow patterns associated with barrier effects, the wind data were taken from the sounding closest to the image time with priority given to earlier soundings when the image time occurred mid-way between soundings. Unfortunately, only mandatory level winds were available for the soundings. Therefore, 850 mb winds were, for the most part, considered representative of the above inversion wind flow. It was occasionally necessary to use 700 mb winds to avoid conflict with the inversion layer. The availability of only mandatory level winds also prevented more detailed above inversion wind and wind shear calculations.

8. Below Layer Stability

The lapse rate between the surface and the inversion base defines the below layer stability. Calculations for this variable were identical to those for inversion strength, except that the levels used were the surface and the inversion base.

9. Above Layer Stability

Above layer stability was calculated as the lapse rate between the top of the inversion layer and a point on the individual sounding which was between 200-250 mb above the top of the inversion. ΔZ was found using Eqn. 3.2 and ΔT was taken from the sounding temperatures. This variable was calculated for a representative sample of eight cases.

IV. RESULTS AND CONCLUSIONS

A. RESULTS

Once the data collection and variable calculation process was completed, five types of mesoscale island barrier effects emerged. These types, as listed in Chapter 2, are:

1) von Karman vortices
2) single plumes
3) transitions from von Karman vortices to single plume
4) calm sea streaks
5) ship wakes

The wind flow and atmospheric structure as evaluated from the available data are now discussed for these different barrier phenomena.

1. von Karman Vortices

An intense, capping inversion characterizes the six von Karman vortices cases. Sounding profiles for these cases, shown in Fig. 4.1, display a sharp temperature rise over a relatively small height change giving values for inversion strength which range from 10 to 29 °C/km (see Table 4). For ease of comparison, the soundings in Fig. 4.1 have been slightly shifted so that the surface temperature is the same for all cases. In no other type are the soundings so similar in shape, particularly near the level of the inversion. Inversion height values in Table 4 show that the inversions occur at less than 600 m in elevation. For Guadalupe Island, this elevation is 500 m below the island's highest point of 1300 m. Thus, the inversion base is located approximately halfway up the island. With the exception of some of the calm sea streak cases, these heights were the lowest found for the barrier effects types. The von Karman vortices cases also show the smallest range of inversion thickness, 380-620 m, among the case types (see Table 4). Thus, this type of barrier effect can be characterized as having a very strong inversion (> 10 °C/km) which is located below the highest elevations of the barrier island and whose inversion layer thickness is relatively small (< 620 m).

Previous studies of von Karman vortices have tended to establish that an inversion exists but little descriptive data are presented. The largest amount of information from these studies is available for inversion heights. In Chopra and

Hubert (1965), the inversion is described as strong and occurring at a height of 800 m, which is approximately half the height of the island producing the vortices (Madeira Island). Using the sounding presented in a figure from their article, calculations for inversion strength and thickness yield values of 47.3 °C/km and 137.3 m. The extremely thin inversion layer, and a ΔT of 6.5 °C across the layer, produce this very large inversion strength value. However, these two values are subject to error from measuring temperatures and pressure levels on a very small figure. In another von Karman case, Zimmerman (1969) reported inversion strength of 7.5 °C/km, inversion height of 1600 m and inversion thickness of 400 m. The inversion strength is below the range found in this study (> 10 °C/km) and the inversion thickness is within the range given above. The inversion height appears significantly higher than the values found for Guadalupe (< 600 m), but is actually less than half the 3720 m height of the island (Tenerife) in his study. Tsuchiya (1969) reported an inversion height of 1510 meters in his study of vortices in the lee of Cheju Island. Since Cheju island is 1950 m high, this inversion is located at an elevation of about three-quarters of the island's highest point. Tsuchiya describes the inversion as being strong, but no numerical value is presented and the accompanying figure is too small to accurately measure values and calculate inversion strength and inversion thickness. The same situation applies to the soundings contained in Thomson *et al.* (1977). The authors stated that the inversion height is 1000 m but did not discuss the strength or thickness of the inversion. Several islands of the Aleutian chain were examined in the study and all of these islands which produced von Karman vortices were above 2000 m elevation. As in other cases, the inversion occurs mid-way up the mountains forming the island barriers. Comparison of these various studies indicates that von Karman vortices are associated with inversion whose heights are approximately half to three-quarters of the elevation of the barrier island.

Cases of the von Karman vortices divide into two groups with respect to surface winds and barrier diameters. One group contained three cases with northerly wind flow with speeds of 5-10 kt. This low wind flow is associated with smaller barrier diameters of 10-14 km for Guadalupe. Cases with moderate winds of 20-30 kt from the northwest formed the second group. Due to the elongated shape of Guadalupe, the moderate wind cases have diameters of 10-25 km depending on the specific wind direction. Tables 3 and 4 contain these wind and island diameter values.

The association of low winds with smaller diameters and moderate winds with somewhat larger diameters, produces a wide range of Reynolds numbers for these cases. In Chapter 2, Eqn. 2.2 established the theoretical relationship between the wind flow and barrier diameter through the Reynolds number. However, effects of eddy viscosity are also included in this parameter. Based on Atkinson's (1981) compilation of previous von Karman vortices cases (Table 1), a mean value for eddy viscosity of 1.63×10^3 m^2 s^{-1} was found. Using this value for eddy viscosity and wind flow and barrier diameter values from Tables 3 and 4, calculations of Reynolds number were made for several Guadalupe Island barrier effect cases. The Reynolds numbers from these calculations are contained in Table 5. For the three low wind cases (S-4, S-8 and S-9), the Reynolds numbers range from 30 to 43, which are at or below the lower end of the range of $40 < Re < 1000$ presented by Chopra (1973). The moderate wind cases (F-13, F-15 and F-17) have Reynolds numbers ranging between 79 and 115, which are within the accepted range of values.

2. Single Plumes

In contrast to the sharply defined profiles of the von Karman vortices cases, the profiles for the four single plume cases (Fig. 4.2) show higher, weaker and thicker capping inversions. Comparison shows the inversions of the plume profiles to have smaller temperature increases over greater vertical distances than those of the von Karman vortices. As shown in Table 4, these plume profiles give higher inversion thickness values (700-1200 m) and coupled with smaller inversion layer ΔT values, result in a lower inversion strength range of 1-10 °C/km. The height of the inversion base is also slightly higher, having a range of 400-800 m but, still remains below the top of the island. Plume cases show the same surface wind flow (northwesterly at 20-30 kt) as the von Karman vortices cases with moderate winds. With this flow the barrier diameters are nearly the same for both barrier effect types (see Tables 3 and 4). Thus, the plume cases are characterized by low inversion strengths and thicker inversions, and by wind flows, barrier diameters and inversion heights similar to those of von Karman vortices.

The plume case Reynolds numbers of 73 and 110 (see Table 5) are above the range ($Re < 65$) proposed in Chapter 2. These values are also within the accepted range (40-1000) for von Karman vortices. Thus, the Reynolds number fails as a parameter to differentiate between plume and von Karman vortex phenomena as suggested by the study of Tsuchiya (1969). A search of the literature did not locate other plume cases for comparison.

3. **Transitions from von Karman Vortices to Plumes**

Profiles for the two transition cases, shown in Fig. 4.3, display similarity to both plume and von Karman vortices. At the inversion base, the temperature increases rapidly but the rate of rise decreases quickly, giving a more gradual slope to the profile. The initial rapid temperature rise is characteristic of the von Karman vortices profile, but the more gradual slope resembles that of plume cases. This gradual slope results in inversion strengths of 3-8 °C/km. As shown in Table 4, these inversion strengths are within the plume case range of values (1-10 °C/km). The inversion thickness values were also within the plume range. However, the inversion heights are higher (900-1000 m) than those of the plume cases. Surface wind flows were again in the same range (20-30 kt) as winds of the plume and moderate wind von Karman vortices cases. Values for the above variables are contained in Table 4. With the inversion occurring at higher elevations, the barrier diameter is reduced to 7 km at the 1000 m elevation (see Table 3). The Reynolds numbers for the transition cases (44 for F-10 and 70 for F-14) are less than the plume case values but are within the accepted von Karman vortices range of 40 to 1000. The similarity between the transition and plume cases is not surprising, considering that at the image time of the transition cases, plume barrier effects had already been established in the lee of the barrier island.

Previous studies have not addressed the transition type of barrier effect; however, the slight differences in the transition case variables suggests a possible sequence of events for the formation of this barrier effect. Initially, a von Karman vortex street forms in the lee of the barrier island. This street arises due to a strong capping inversion with a low inversion base. The surface wind flow remains constant through this and subsequent phases of the transition. At some later time, the inversion layer begins to rise and its thickness increases. Upward vertical motion generated by solar heating of the island or synoptic-scale upward motion are possible causes of this change in the inversion layer. With a larger inversion thickness, the inversion strength is reduced. With a steady wind flow, the smaller inversion strength and the smaller barrier diameter change the vortex street into a single plume.

4. **Calm Sea Streaks**

The seven cases of calm sea streaks divide into three categories based on the shapes of their sounding profiles. Four cases resemble von Karman vortices profiles, one case is similar to the single plumes, and two cases show different profiles altogether. The primary difference between the soundings for the calm sea streaks and

the other barrier effect types they resemble (plumes and von Karman vortices) is the lower moisture content of the boundary layer between surface and inversion.

For those cases with profiles similar to von Karman vortices, the three inversion variables are nearly the same, as shown in Table 4. The range of inversion strengths of 11-25 °C/km is within the 10-29 °C/km range of the von Karman cases. For the calm sea streak cases, the inversion heights are slightly lower (100-400 m), and the inversion thickness range of 350-800 m is slightly larger than the corresponding von Karman vortices case values of 300-600 m for inversion height and 300-650 m for thickness. These characteristics suggest stronger subsidence in these cases. This subsidence and lower inversion height does contribute to the dryness below the inversion through entrainment. This dryness is represented by dew-point depression as shown in Fig. 4.4. In contrast, Fig. 4.5 shows the vertical profiles for a representative von Karman vortices case. In this figure, the dew-point depression is considerably smaller which indicates more moisture in the lower levels of the atmosphere.

Imagery of calm sea streak cases with soundings similar to von Karman vortices shows oscillations in the calm sea streaks. These patterns could indicate an interaction between the sea surface and von Karman vortices in the atmosphere above the surface. Chopra (1973) proposed that the eddies in the sea surface in the lee of Hawaii were caused by atmospheric vortices. These vortices were shown to exist by Nickerson and Dias (1981) which supports the idea that sea-surface patterns, such as calm sea streaks, can be reflections of atmospheric eddies, like von Karman vortices.

In one calm sea streak case, the sounding profile appears similar to the plume type profiles. Its inversion strength value is 5.5 °C/km which is in the middle of the plume range (see Table 4). This case has an inversion height of 323 m and an inversion thickness of 272 m. These values are lower and smaller than the corresponding ranges found in the plume cases, again indicating stronger subsidence in this situation. With only one calm sea streak case, the significance of these differences is difficult to determine. As seen in Fig. 4.6, the boundary layer is significantly drier for this case also.

Soundings for the remaining two calm sea streak cases show profiles with high and weak inversions. The shapes of the two profiles (Fig. 4.7) do not show a strong resemblance to the profiles of other island barrier effect types. As shown in Table 4, the inversion strengths are within the plume type range, being less than 10 °C/km. However, the inversion heights are 300 m above the highest elevation of the barrier

islands and the inversion thicknesses are relatively thin, being less than 300 m. The high height of the inversion base is explained by the fact that in both cases the islands are located in tropical western oceans. In the tropics, the boundary layer inversion rises to the west as one moves from the eastern to the western tropical ocean region. Riehl (1954) states that climatologically the strongest and lowest trade inversions occur in the eastern oceans with the inversion ascending to the west.

It is interesting that even with a high, weak inversion, a pronounced surface calm zone develops. Another factor in this phenomenon is the presence of weak winds aloft. In all but one of the calm sea streak cases, the winds above the inversion are 10 kt or less (Table 4 and Fig. 4.8). This suggests that the role of the island barrier is more than that of blocking the flow. The island disrupts the inversion so that the dry low momentum air is mixed down to the surface layer. A long sea streak is a probable indicator of weak winds aloft as well as a drier boundary layer.

5. Ship Wakes

The sounding profiles for the four ship wake cases (Fig. 4.9) show inversion base heights above the barrier island. These heights range between 150 and 400 m above the islands' highest elevations (see Tables 3 and 4). Edinger and Wurtele (1972) reported a ship wake case for San Nicolas Island. For this case, the associated sounding showed an inversion height of approximately 300 m above the island. The inversion strength range of 2-14 °C/km encompasses both very weak and moderately strong inversions. As shown in Table 4, the ship wake type also possesses the widest range of inversion thickness values. These values range between 90 and 800 m. The surface winds were low to moderate (10-22 kt), but the above inversion winds were approximately 50 kt for these cases. Ship wakes are the only cases with such strong vertical velocity shear. The high, stable inversions of the ship wake cases tends to support the gravity wave model proposed by Edinger and Wurtele, but additional cases are needed for verification.

6. Other Results

The remaining variables, above inversion winds (except as noted above) and above and below layer stabilities, showed little effect on the formation or maintenance of the island barrier effects. Calculations show that the mean below inversion stability is -9.3 °C/km which is essentially the same as the adiabatic lapse rate. Similarly, the above inversion stabilities show values less than the adiabatic lapse rate, with the mean value for the eight sample cases being less than -6 °C/km. The above inversion wind

speeds vary considerably among the cases and show little influence on the island barrier effects, except for the ship wake and calm sea streak cases. The wind shear relationship between the surface and above inversion winds (shown in Fig. 4.8) also shows considerable variability in both direction and speed.

B. CONCLUSIONS

The results of this study indicate that there are three key variables which synoptically characterize the mesoscale island barrier effects. The three variables; inversion strength, inversion height and inversion thickness, are interrelated. For example, when subsidence is strong, the inversion lowers and the inversion layer is thinner with a larger inversion strength. When upward vertical motion occurs, the inversion height rises, the inversion layer thickness increases and its strength decreases.

Based on these three variables, the mesoscale island barrier effects can be characterized. When a capping inversion is strong and has a small thickness and is located at a height approximately half that of the highest elevation of the barrier island, von Karman vortices form in the lee of the island. Plume and transition cases occur when the inversion is thicker and weaker than those inversions found in von Karman vortices cases. When the inversion is above the highest elevation of the island and has thickness and strength values in the range of either plumes or von Karman vortices and a strong velocity wind shear exists, then ship wakes form.

The calm sea streaks are mesoscale island barrier effects in which either boundary layer vertical motion is absent or the below inversion moisture content is insufficient to form the cloud patterns associated with plumes and von Karman vortex streets. The oscillations in the calm sea streaks indicate the presence of barrier effects eddies in the atmosphere above the sea surface. The western ocean calm sea streak cases display the higher trade wind inversions prevalent in the tropical western ocean regions and light winds aloft.

The Reynolds numbers for von Karman vortices cases are in general agreement with earlier studies. However, the Reynolds numbers for plume and transition cases give a range which are inconsistent with theory and previous studies. This inconsistency could stem from several sources; significant differences between the actual eddy viscosities and the mean value, inaccurate measurements of wind flow velocity or barrier diameter, or surface winds not being representative of the actual wind flow near the inversion base. Because of the range in the Reynolds number

values and since values for eddy viscosity cannot be easily found from routine synoptic observations, use of the Reynolds number as a island barrier effects characterization parameter does not appear feasible.

The goal of developing a classification scheme for mesoscale island barrier effects appears premature at this point. While this study determined a number of key features of differing barrier effects phenomena, the generalization of these results must await additional confirming cases.

V. RECOMMENDATIONS

In this study, only 23 cases describing five categories of mesoscale island barrier effects were examined. The collection of additional cases is required to verify the synoptic characterizations presented and to further investigate the relationships between the synoptic variables and island barrier effects. The need for additional cases is particularly true for the transition from von Karman vortices to plume, ship wake and calm sea streak case types. For example, how the higher inversion of the western tropical ocean and the barrier island interact to form calm sea streaks remains unclear. Further study of the island barrier effects may result in better descriptions of their formation processes.

Another area for future work is the investigation of mesoscale barrier effects in the lee of isolated mountain peaks. In the barrier effects image collection of Dr. Robert Fett there are several cases of plume-like clouds extending from isolated peaks located in Central America. Revell (1983) reports cases of von Karman vortices produced in the lee of Mt Egmont, which is an isolated mountain peak located on the Northwest coast of New Zealand. These images indicate that barrier effects do form in the lee of single peaks, opening another area for study.

This study examined five types of island barrier effects prevalent in satellite imagery. Several other types of related mesoscale/microscale phenomena also are present in imagery and should be included in future studies of barrier effects. Among these phenomena are corner effects in sunglint patterns, microscale cloud lines along the edges of calm sea streaks and gravity wave packets occuring along coastal zones. Another area for future study is the microscale circulation patterns at the edges of mesoscale island barrier effects. The presence of clear areas within von Karman vortices implies some microscale vertical circulation and entrainment of drier air into the vortex street.

Once a satisfactory set of descriptive synoptic variables and/or parameters, which characterize mesoscale island barrier effects, is established, research into applying this knowledge to nowcasting and forecasting techniques is required. In order to make forecasts of island barrier effects, better numerical weather prediction models are needed. These models must be able to predict detailed vertical structure of the

atmosphere so that the inversion strengths, thicknesses and heights can be forecast. With the increasing availability of satellite imagery to naval units, techniques in characterizing phenomena present in this imagery and using these characterizations in forecasting will become more valuable in assisting operational Naval Oceanographers in supporting naval operations.

APPENDIX

TABLES AND FIGURES

TABLE 1

SUMMARY OF VORTEX STREET PARAMETER VALUES

Calculated values that characterize atmospheric mesoscale vortex streets and associated flow. After Atkinson (1981).

Location	h/a	Propagation speed ($m\,s^{-1}$)	Period of vortex pair formation ($=1/j$, where j is frequency of formation) (h)	Eddy viscosity ($m^2\,s^{-1}$)	Reynolds number	Strouhal number
Pavlof Volcano†	0.38	7.5	2.4	1.5×10^3	120	0.21
Shishaldin Volcano†	0.47	7.5	2.8	1.8×10^3	183	0.32
Pogromni Volcano†	0.60	7.5	1.9	1.2×10^3	112	0.19
Mount Vsevidof†	0.47	7.5	2.8	1.8×10^3	97	0.17
Kiska Island†	0.30	7.5	3.1	1.9×10^3	100	0.16
Tenerife Island‡	0.39	5	6.8	1.2×10^3	210	0.21
Gran Canaria Island‡	0.39	5	7.3	1.3×10^3	170	0.17
Madeira Island‡	0.39	5	12.0	2.2×10^3	150	0.15
Cheju Island, Korea§	0.33	7	4.4	1.8×10^3	180	0.20

† *Source*: Thomson *et al.* (1977).
‡ *Source*: Zimmerman (1969).
§ *Source*: Tsuchiya (1969).

TABLE 2

LIST OF CASES

Case #	Location	Date	Image Time (GMT)	Image Number	Data Available
A. Satellite Imagery Cases					
F-1	Guadalupe	08 Apr 74	1853		Yes
F-2	Guadalupe	21 May 74	1631		Yes
F-3	Guadalupe	10 Apr 74	1816		Yes
F-4	Guadalupe	17 May 77	1933		Yes
F-5	Martinique	10 May 79	1501		Yes
F-6	Guadalupe	12 Jul 79	1835		No
F-7	Guadalupe	09 Jul 79	1645		Yes
F-8	Guadalupe	10 Jul 79	1627		Yes
F-9	Guadalupe	02 Apr 79	1828		Yes
F-10	Guadalupe	15/16 Jun 73	2018/0000		Yes
F-11	Not used				
F-12	Guadalupe	16 Jun 80	1856		No
F-13	Guadalupe	15 May 74	1918		Yes
F-14	Guadalupe	17 May 74	1630		Yes
F-15	Guadalupe	25 Aug 76	1544		Yes
F-16	Socorro	11 Apr 74	1758		No
F-17	Guadalupe	08 May 73	1920		Yes
F-18	Canary Is.	18 Jul 77	1132		No
F-19	Faeroes	23 Jun 75	0829		Yes
M-1	Guadalupe	10 Mar 86	1830		Yes
B. Manned Spaceflight Photograph Cases					
S-1	Sirri Island	07 Mar 83	08-09	S-6-45-068	No
S-2	San Nicolas	16 Jul 75	2225	AST-14-878	Yes
S-3	Antipodes	17 Dec 73	0020	SL4-137-3668	Yes
S-4	Guadalupe	04 Jul 82	13-14	STS-4-38-866	Yes
S-5	Cape Verde	15 Apr 85	1256	51D-42-018	Yes
S-6	Aleutians	04 Aug 85	0547	51F-35-028	Yes

TABLE 2

LIST OF CASES (cont'd.)

Case #	Location	Date	Image Time (GMT)	Image Number	Data Available
S-7	S. Sandwich	12 Oct 84	1959	S17-45-113/114	No
S-8	Guadalupe	01 May 85	1828	51B-35-094/095	Yes
S-9	Guadalupe	17 Jun 85	1619	51G-31-014/015	Yes
S-10	Canary	31 Aug 85	0822	51I-44-001/002	No
S-11	Guadeloupe	04 Feb 84	15-17	41B-32-1308/1309	Yes

Notes: 1) Satellite images identified by date and time.
2) Photographs with range of times (e.g. 08-09Z) could only b placed within the period of a single orbit, exact photogra time not recorded.

TABLE 3

BARRIER ISLAND DIMENSIONS

Barrier Island	Highest Elevation (m)	Barrier Diameter at Height of Inversion Diameter (km)	Elevation (m)	Wind Direction (deg)
Guadalupe	1300	13.5	500	360
		13.5	500	330
		11.5	800	330
		7.0	1000	330
		25.0	500	300
Antipodes	366	7.0	200	270
		15.0	200	360
Cape Verde Islands				
Brava	976	6.0	200	360
Fogo	2829	21.0	200	360
Faeroes	882	46.0	200	360
		48.0	200	270
Guadeloupe	1467	42.0	200	090
Martinique	1397	43.0	200	090
San Nicolas	271	15.0	200	360
		7.0	200	090

TABLE 4

SYNOPTIC VARIABLE RESULTS SUMMARY

Case #	Location	Inversion Height (km)	Inversion Strength (C/km)	Inversion Thickness (km)
A. von Karman vortices				
S-4	Guadalupe	347.5	17.365	598.9
S-8	Guadalupe	354.8	19.070	382.8
S-9	Guadalupe	304.2	29.244	543.7
F-13	Guadalupe	469.5	10.319	610.5
F-15	Guadalupe	372.6	11.354	616.5
F-17	Guadalupe	554.3	17.290	462.7
B. Plume				
F-3	Guadalupe	727.7	1.834	1199.3
F-4	Guadalupe	781.4	1.718	1164.1
S-5	Cape Verde	611.8	4.577	830.2
S-2	San Nicolas	412.1	8.995	722.6
C. Transition - von Karman vortices to plume				
F-10	Guadalupe	939.7	7.740	930.2
F-14	Guadalupe	998.5	3.370	1097.6
D. Calm sea streaks				
F-1	Guadalupe	389.3	11.817	736.2
F-2	Guadalupe	318.6	13.043	368.0
F-7	Guadalupe	101.6	25.061	371.1
F-8	Guadalupe	101.7	14.994	800.3
F-9	Guadalupe	323.2	5.498	272.8
F-5	Martinique	1768.7	1.841	271.6
S-11	Guadeloupe	3743.4	8.542	163.9
E. Ship wake				
F-19	Faeroes	1081.7	2.032	787.3
M-1	Guadalupe	1467.1	13.989	500.4
S-3	Antipodes	804.6	5.612	89.1
S-6	Aleutians	728.2	10.004	279.9

TABLE 4

SYNOPTIC VARIABLE RESULTS SUMMARY (cont'd.)

Case #	Surface Winds (kt)	Above Inversion Winds (kt)	Below Inversion Stability (C/km)	Relative Humidity (%)
A. von Karman vortices				
S-4	360/08	NA	−8.622	90.6
S-8	360/10	240/12	−6.483	96.7
S-9	360/07	245/8	−13.807	96.7
F-13	320/25	NA	−11.928	87.5
F-15	320/20	290/12	−10.199	77.4
F-17	340/25	330/14	−13.170	93.4
B. Plume				
F-3	320/30	345/24	−10.581	78.8
F-4	320/20	290/18	−11.006	78.4
S-5	050/12	130/10	−14.384	93.6
S-2	260/09	260/06	−13.346	85.0
C. Transition - von Karman vortices to plume				
F-10	340/20	290/14	−10.322	96.6
F-14	320/22	NA	−7.011	78.2
D. Calm sea streaks				
F-1	320/14	230/20	−15.155	93.5
F-2	330/12	345/04	−9.416	90.4
F-7	360/24	290/04	−2.953	82.5
F-8	320/25	280/08	−6.883	79.9
F-9	330/25	345/12	−6.807	38.4
F-5	110/15	075/06	−7.444	79.4
S-11	120/18	175/04	−5.610	64.8
E. Ship wake				
F-19	240/22	245/54	−7.211	89.8
M-1	300/10	250/48	−7.634	96.6
S-3	350/20	NA	−10.813	64.0
S-6	240/12	NA	−2.060	86.9

TABLE 5

REYNOLDS NUMBERS CALCULATED FOR GUADALUPE ISLAND CASES

Case #	Height (m)	Barrier Diameter (km)	Wind (deg/kt)	Reynolds Number
A. von Karman vortices				
S-4	500	13.5	360/08	34
S-8	500	13.5	360/10	43
S-9	500	13.5	360/07	30
F-13	500	14.5	320/25	115
F-15	500	14.5	320/20	92
F-17	500	10.0	340/25	79
B. Plume				
F-3	800	11.5	320/30	110
F-4	800	11.5	320/20	73
C. Transition - von Karman vortices to plume				
F-10	1000	7.0	340/20	44
F-14	1000	7.0	320/22	70

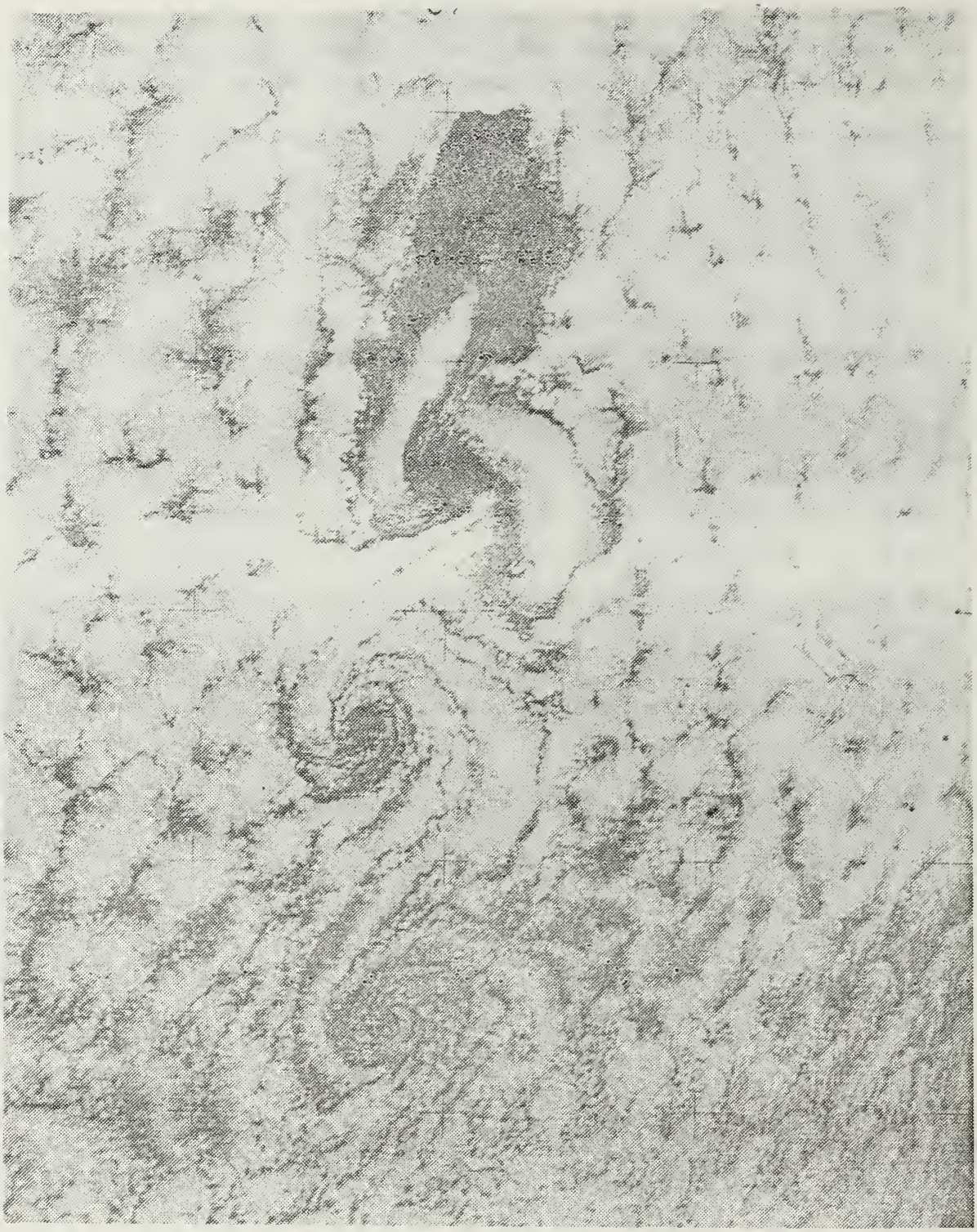

Figure 1.1 Skylab photograph showing von Karman vortices in lee of Guadalupe Island off the coast of Baja California (SL3-122-2497).

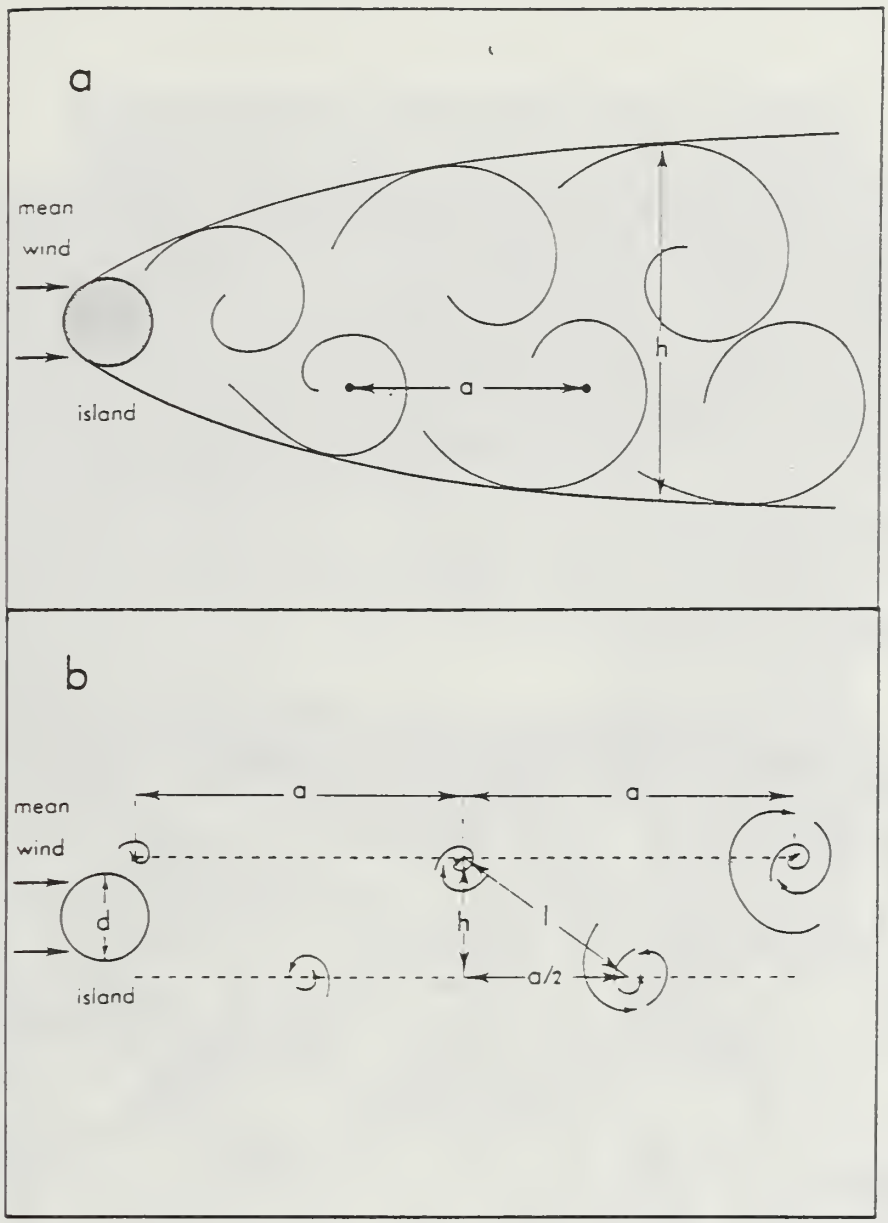

Figure 2.1 Schematic diagram of (a) von Karman vortices leeward of an isolated island and (b) vortex street dimensional variables. After Chopra and Hubert (1975).

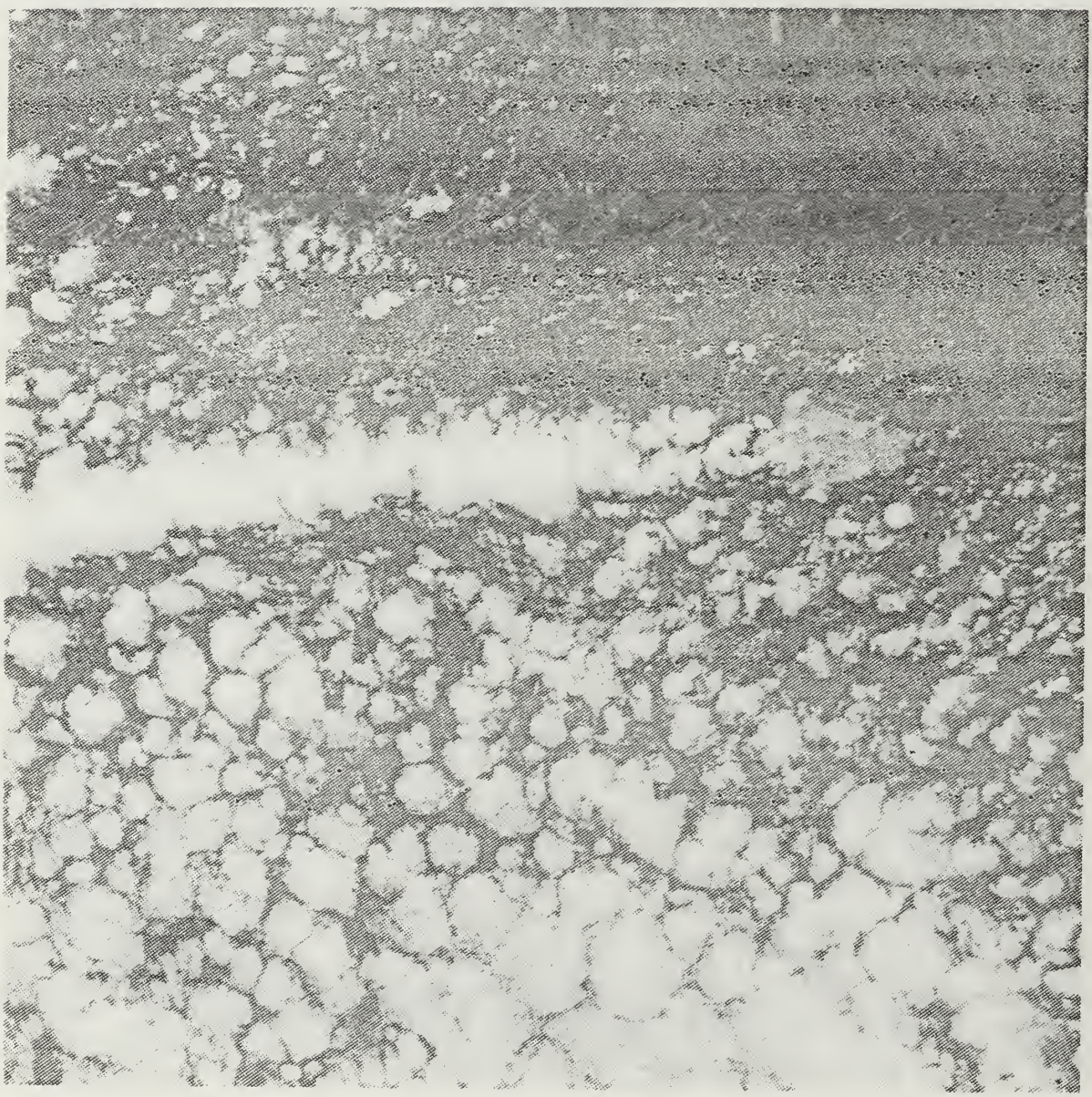

Figure 2.2 Single cloud plume in lee of Sirri Island, Iran taken from space shuttle mission STS-6 (S-6-45-068).

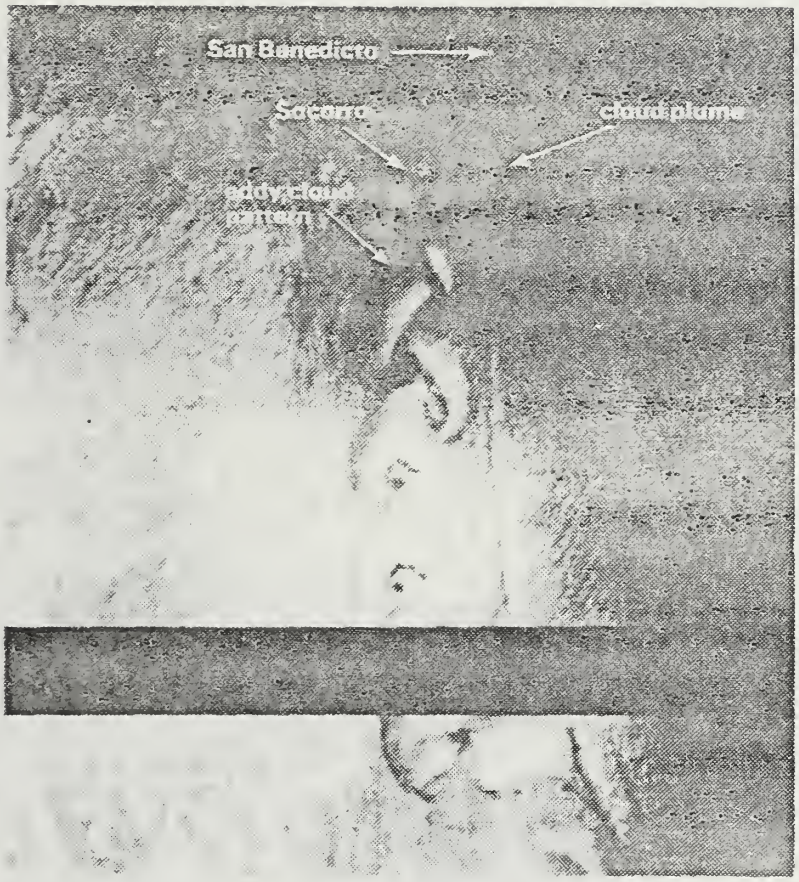

Figure 2.3 1920 GMT DMSP satellite image of 8 May 1973 showing von Karman vortices from Socorro Island and a single cloud plume from San Benedicto Island.

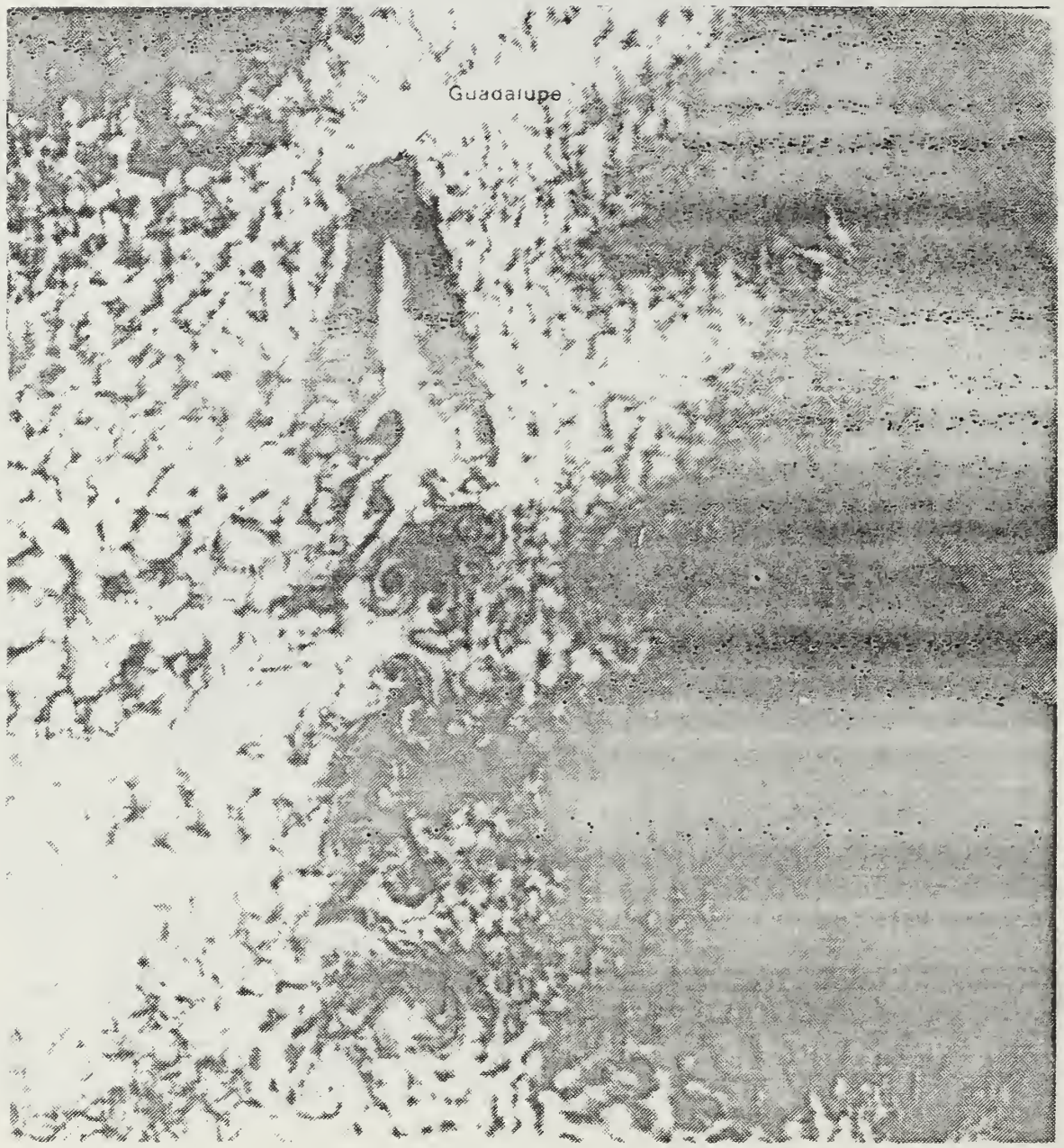

Figure 2.4 2018 GMT DMSP satellite image of 15 June 1973 showing transition from von Karman vortices to single plume.

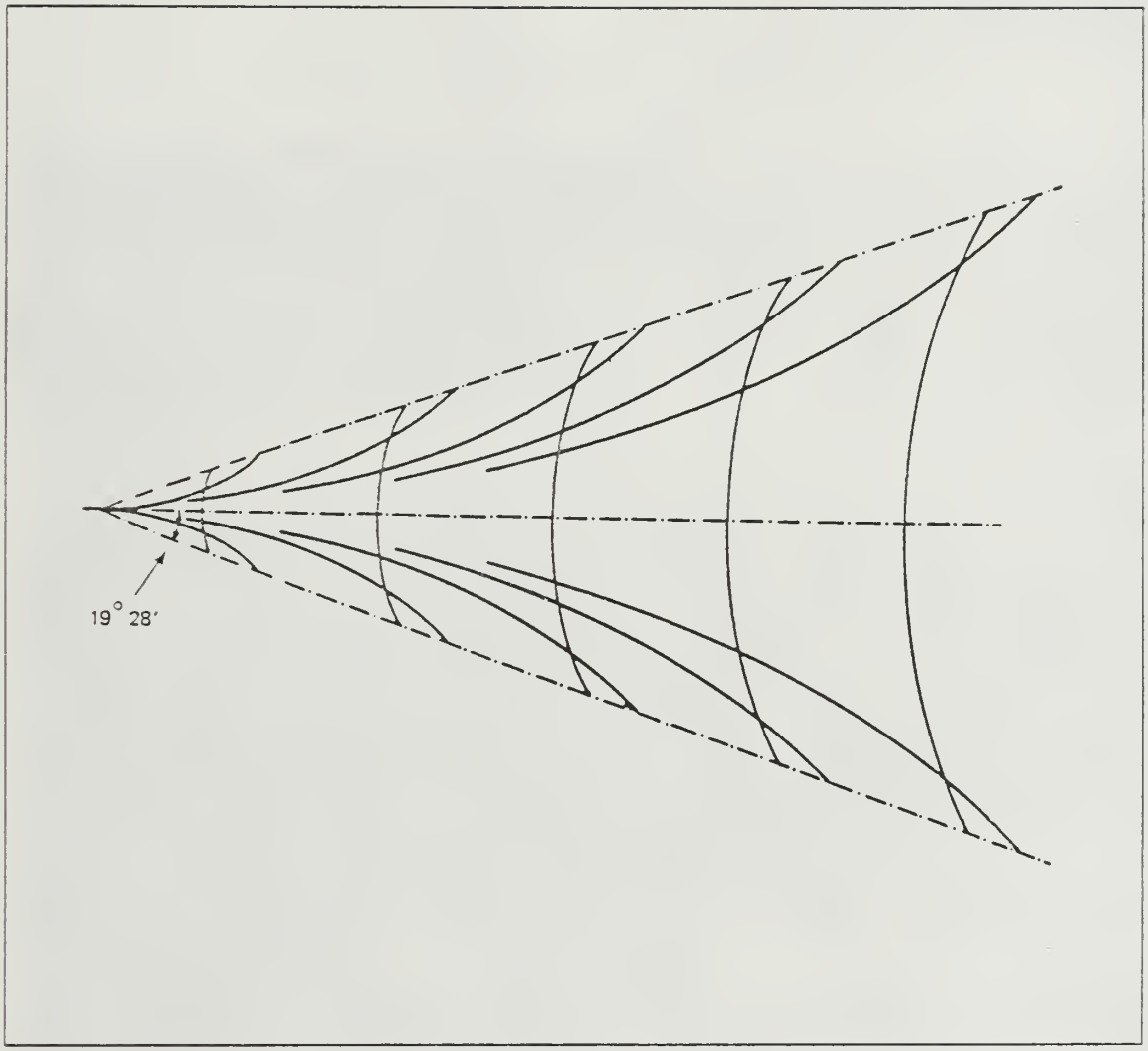

Figure 2.5 Schematic diagram of the theoretical ship wake. Heavy lines denote wave crests. (After Hogner, 1922).

Figure 2.6 Skylab photograph showing ship wake clouds in lee of Antipodes Islands (SL-4-137-3668).

Figure 2.7 Calm sea streaks in lee of Guadeloupe Island (Lesser Antilles) taken from space shuttle mission 41B (41B-32-1308).

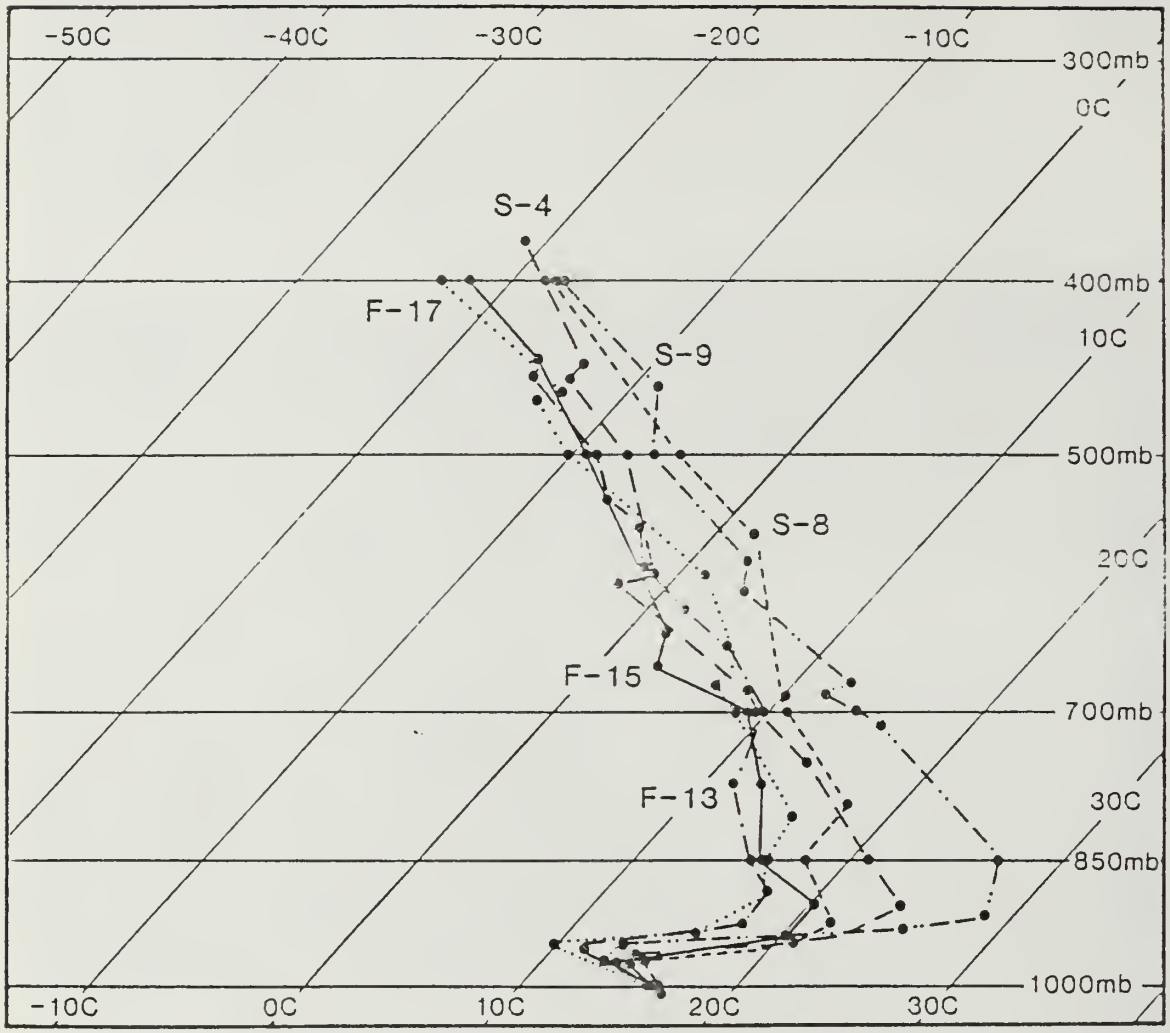

Figure 4.1 Upper-air temperature profiles for cases showing von Karman vortices. Profiles have been shifted to a common surface temperature of 17 °C.

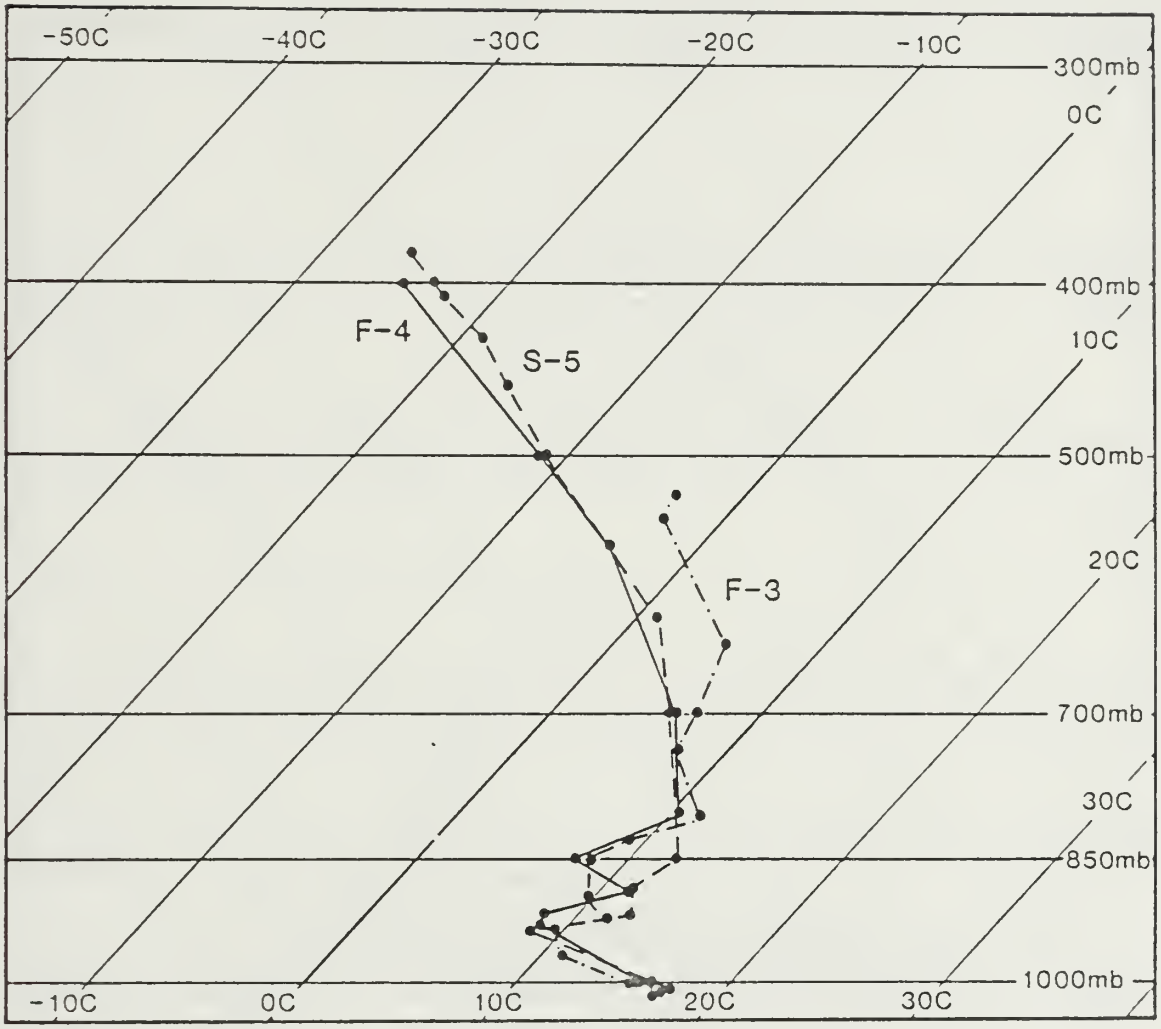

Figure 4.2 Same as Fig. 4.1 but for cases showing single plumes.

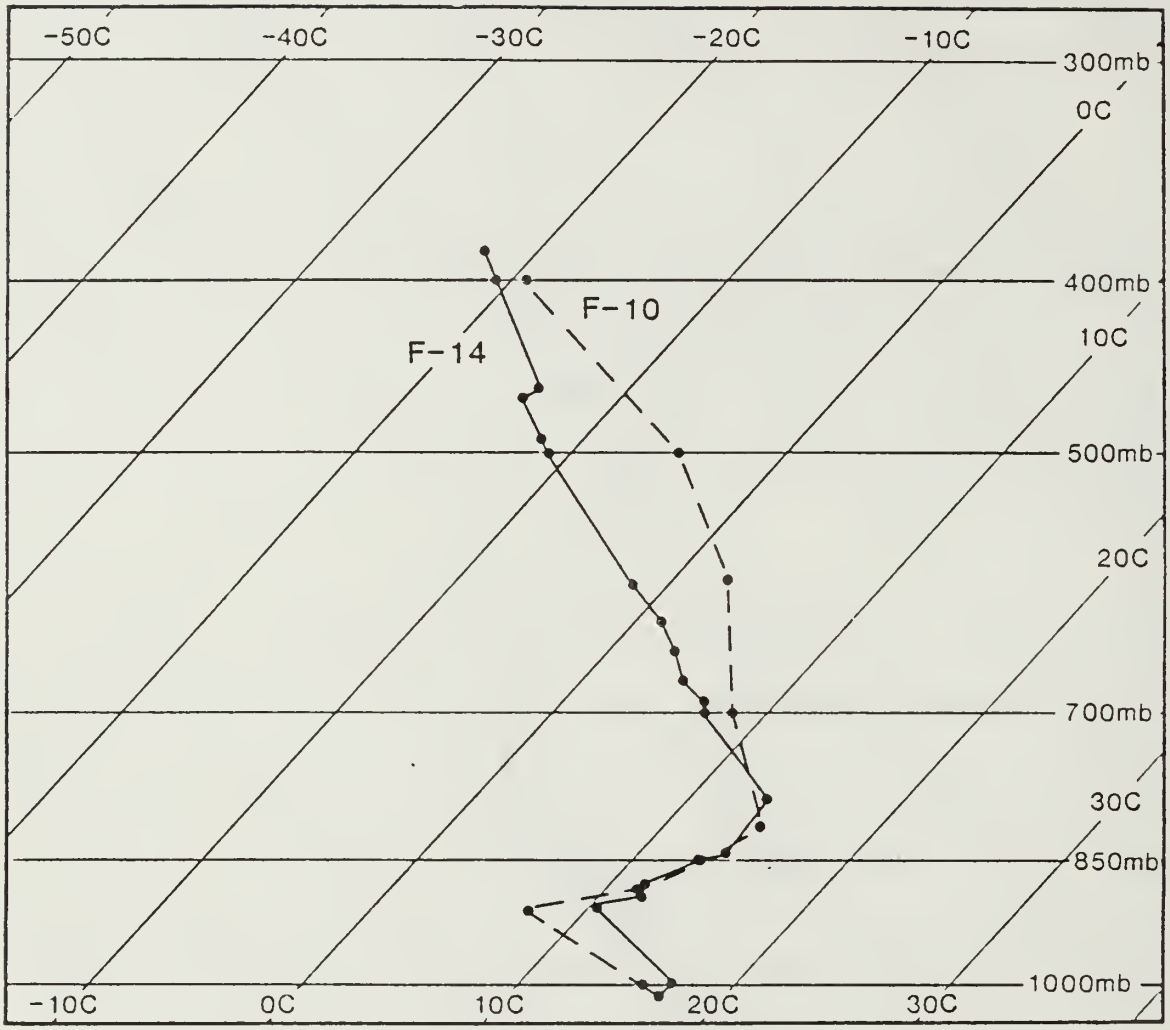

Figure 4.3 Same as Fig. 4.1 but for cases showing transition from von Karman vortices to single plumes.

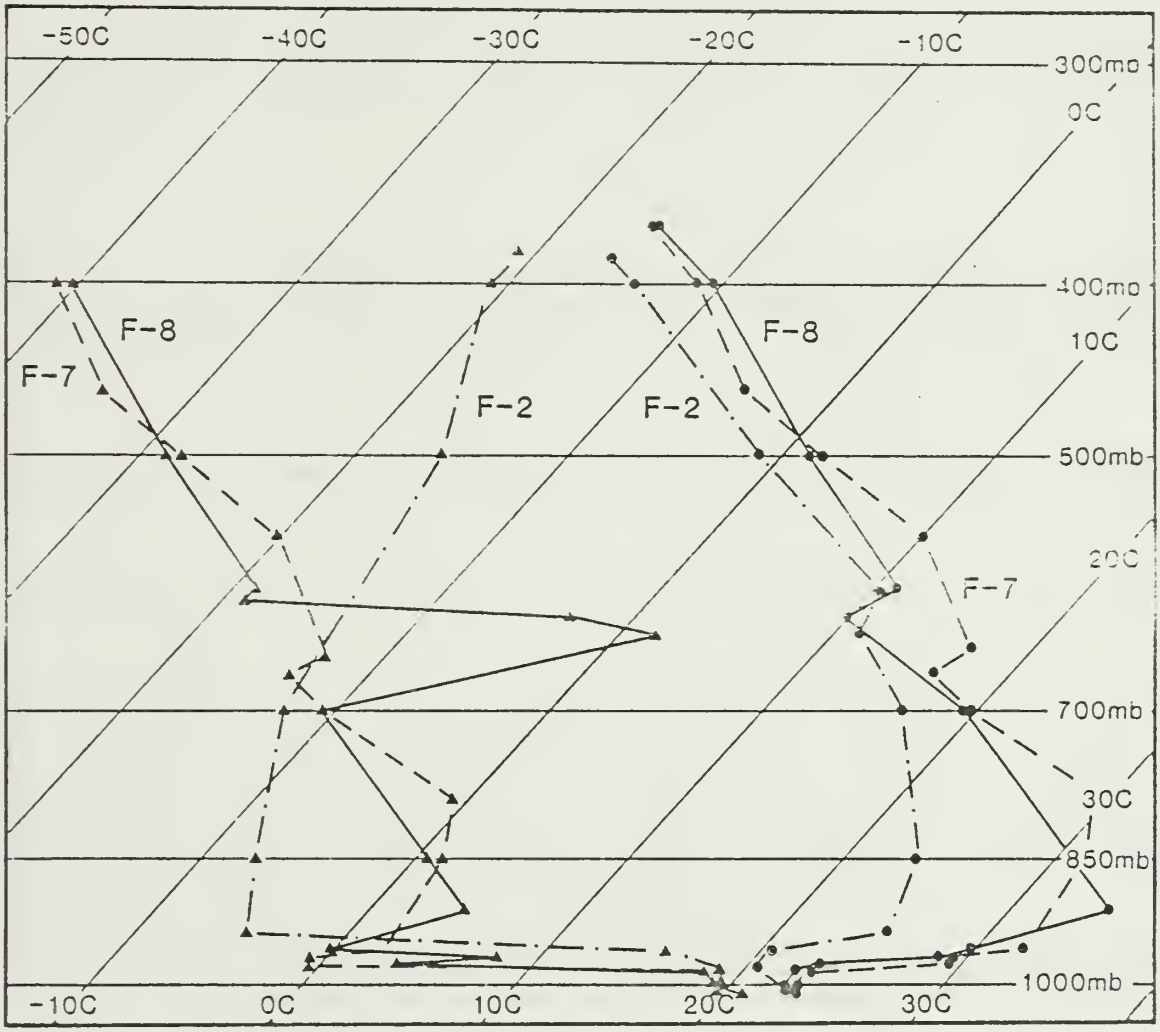

Figure 4.4 Temperature and dew point profiles for calm sea streak cases showing profiles similar to von Karman vortices. Note $T-T_d$ separation below inversion layer.

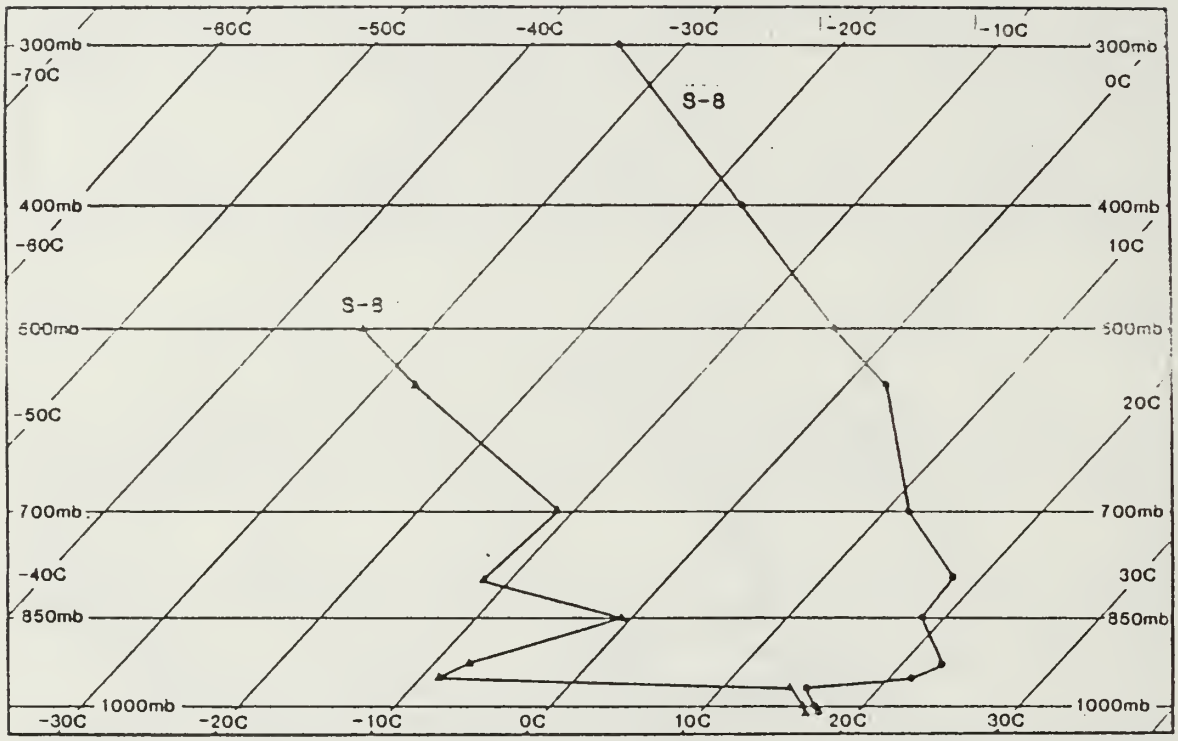

Figure 4.5 Temperature and dew point profile for von Karman vortices case S-8. Dew point depression shows higher moisture in boundary layer as compared to Fig 4.4.

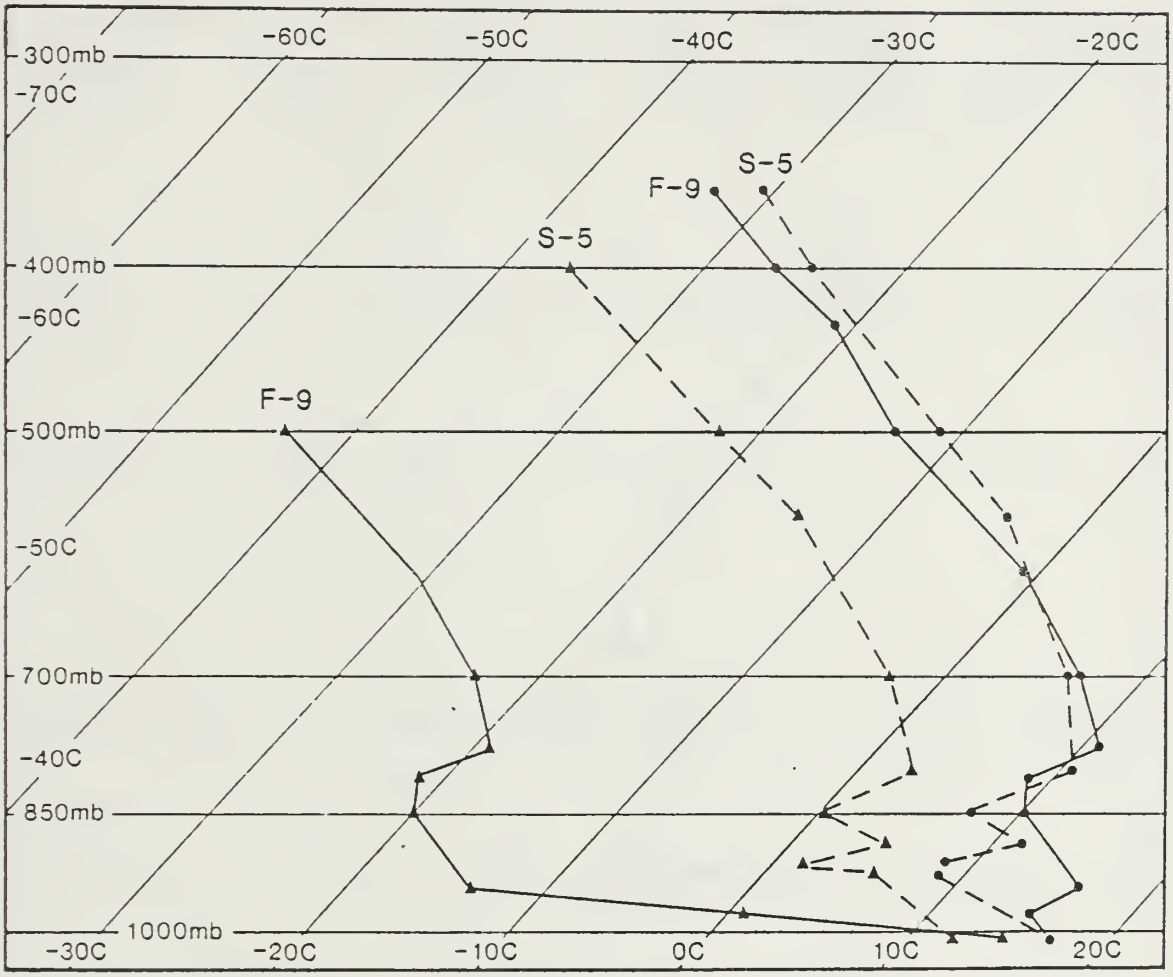

Figure 4.6 Comparison between calm sea streak case F-9, with plume profile and plume case, S-5. Note difference in moisture in boundary layer.

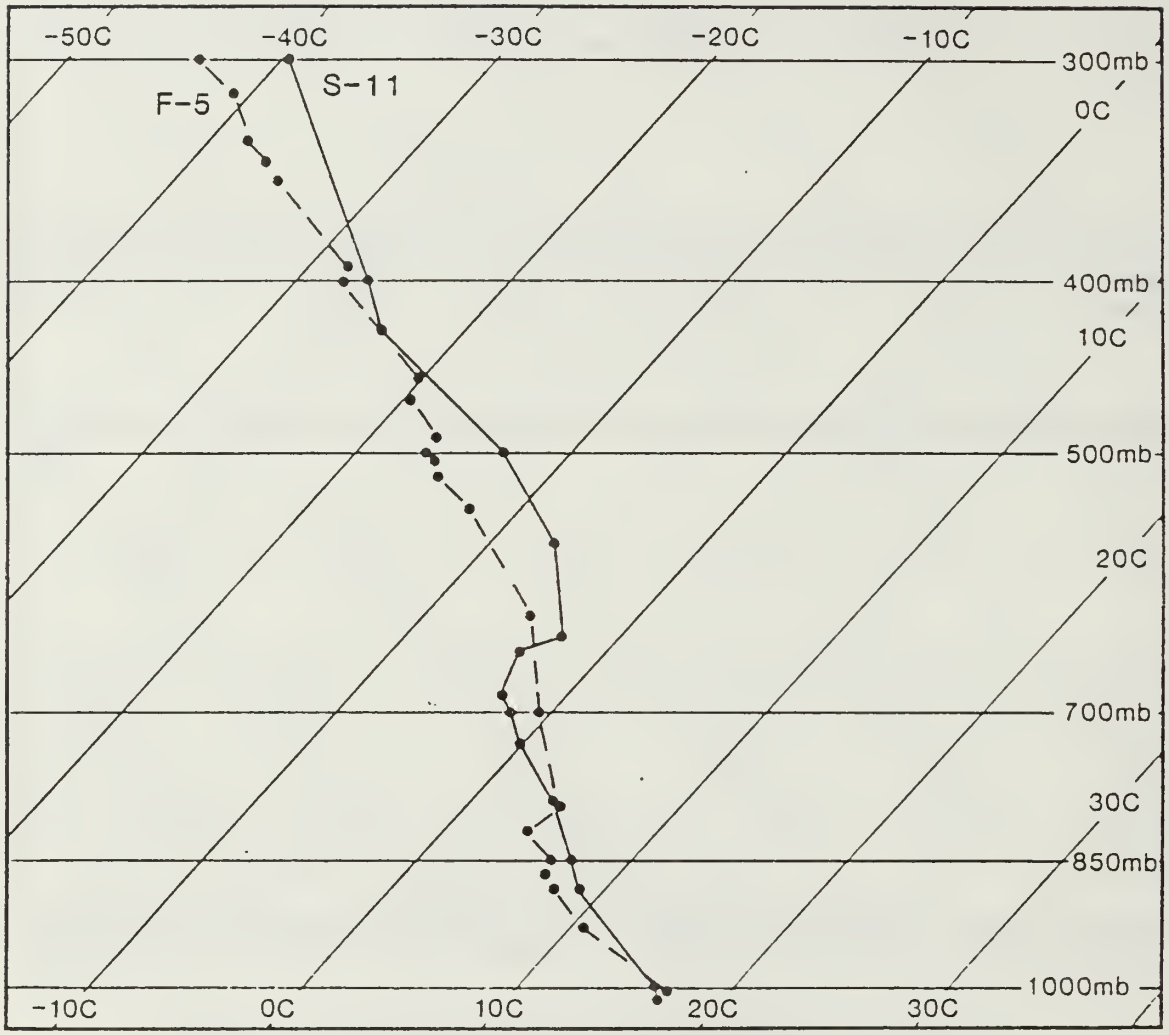

Figure 4.7 Same as Fig. 4.1 but for cases showing tropical western ocean calm sea streaks.

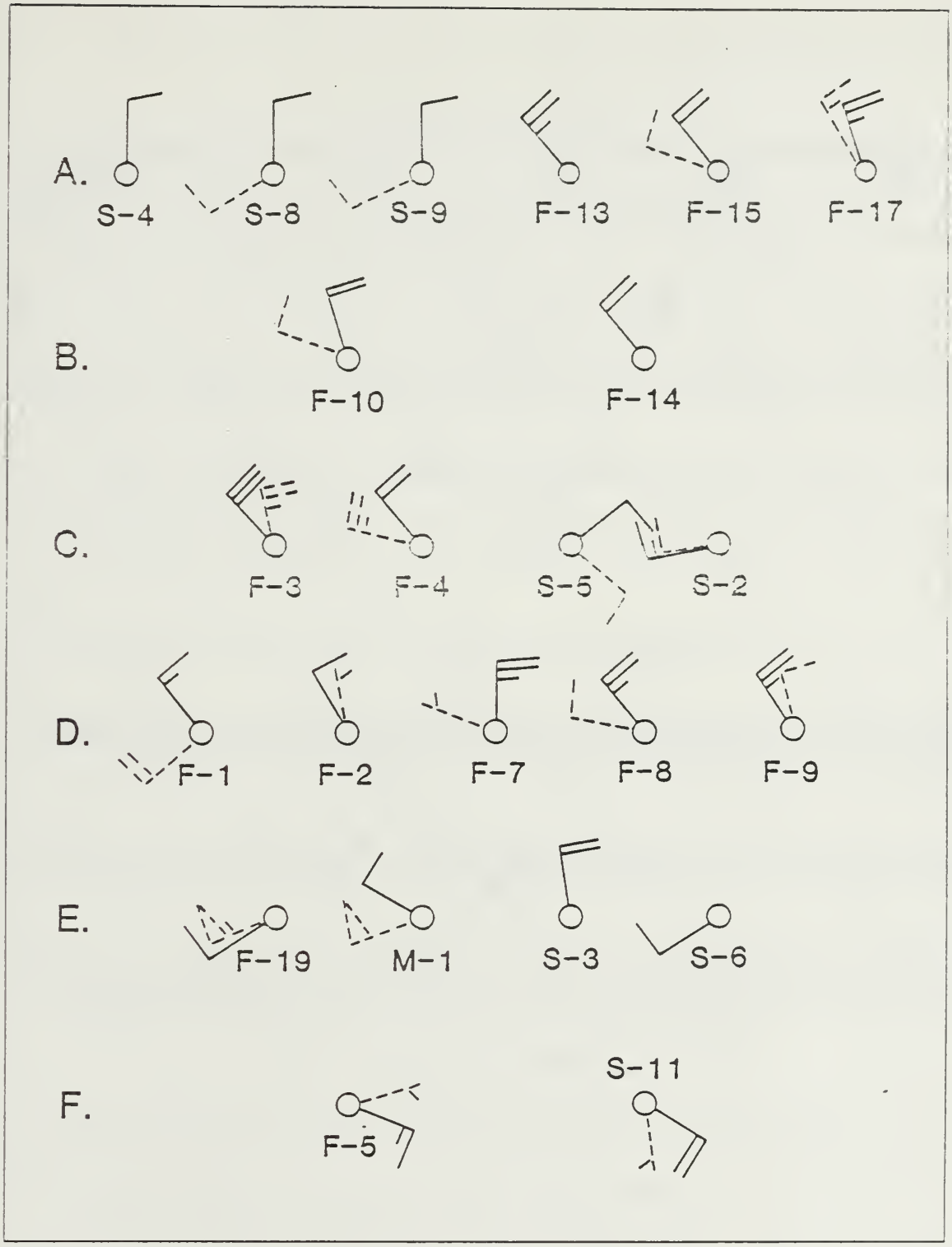

Figure 4.8 Station plots showing surface (solid) and upper air (dashed) winds. A. von Karman vortices, B. transition, C. plume, D. sea streak, E. ship wake and F. western ocean sea streak.

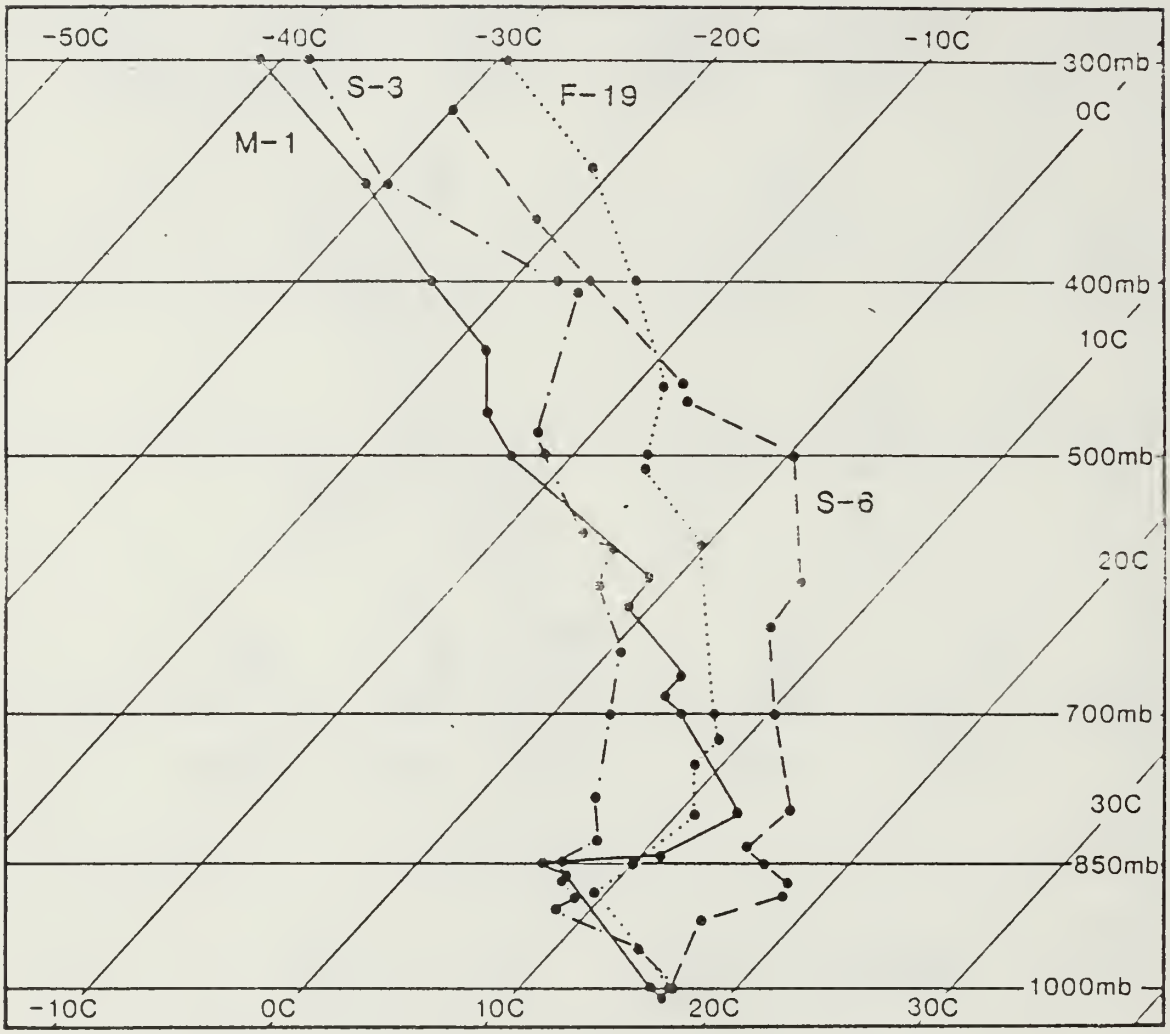

Figure 4.9 Same as Fig. 4.1 but for cases showing ship wake pattern.

LIST OF REFERENCES

Atkinson, B. W., 1981: *Meso-scale Atmospheric Circulations.* Academic Press, London, 495 pp.

Black, P. G., 1978: Mesoscale cloud patterns revealed by Apollo-Soyuz photographs. *Bull. Amer. Meteor. Soc.*, 59, 1409-1419.

Bowley, C. J., A. H. Glaser, R. J. Newcomb and R. Wexler, 1962: Satellite observations of wake formation beneath an inversion. *J. Atmos. Sci.*, 19, 52-55.

Chopra, K. P., 1972: Lin parameter as characteristic of atmospheric vortex streets. *AIAA J.*, 10, 345-347.

_____, 1973: Atmospheric and oceanic flow problems introduced by islands. *Adv. Geophys.*, 16, 297-421.

_____, and L. F. Hubert, 1965: Mesoscale eddies in wake of islands. *J. Atmos. Sci.*, 22, 652-657.

Edinger, J. G., and M. G. Wurtele, 1972: Interpretation of some phenomena observed in Southern California stratus. *Mon. Wea. Rev.*, 100, 389-398.

Fett, R. W., and K. Rabe, 1975: Island barrier effects on sea state and atmospheric moisture as detected by a numerical wave model and sensors of the Defense Meteorological Satellite Program (DMSP). *NAVENVPREDRSCHFAC Tech. Paper No. 18-75*, Naval Environmental Prediction Research Facility, Monterey, CA, 67 pp.

_____, and W. F. Mitchell, 1977: *Navy Tactical Applications Guide, Vol. I: Techniques and Applications of Image Analysis.* NAVENVPREDRSCHFAC Applications Report 77-03. Naval Environmental Prediction Research Facility, Monterey, CA, 110 pp.

Fujita, T. T., and J. J. Tescon, 1977: Mesoscale wake clouds in Skylab photographs. *Skylab Explores the Earth*, NASA SP-380, eds. V. R. Wilmarth, J. L. Kaltenbach and W. B. Lenoir, NASA Lyndon B. Johnson Space Center, Houston, TX, 463-477.

Havelock, T. H., 1950: *Wave Resistance Theory and its Application to Ship Problems.* Society of Naval Architects and Marine Engineers, New York, 352 pp.

Heffter, G. L., 1965: The variation of horizontal diffusion parameters and travel periods of one hour or longer. *J. Appl. Meteor.*, 5, 153-156.

Hogner, E., 1922: A contribution to the theory of ship wakes. *Arkiv fur Matematik, Astronomi och Fysik*, 17, 1-50.

Holton, J. R., 1979: *An Introduction to Dynamic Meteorology.* Academic Press, New York, 391 pp.

Hubert, L. F., and A. F. Krueger, 1962: Satellite pictures of mesoscale eddies. *Mon. Wea. Rev.*, 90, 457-463.

Kelvin, W. T., 1887: On the waves produced by a single impulse in water of any depth, or in a dispersive medium. *Proc. Roy. Soc. (London)*, ser. A, vol. 42, 80-85.

Lin, C. C., 1959: On periodically oscillating wakes in the Oseen approximation. *Studies in Fluid Mechanics Presented to R. von Mises*, Academic Press, New York, 170-176.

Nickerson, E. C., and M. A. Dias, 1981: On the existance of atmospheric vortices downwind of Hawaii during the HAMEC project. *J. Appl. Meteor.*, 20, 868-873.

Ormsby, J. P., 1977: *Mesoscale Cloud Phenomena Observed by Landsat*. NASA Tech. Note TND-8494, Goddard Space Flight Center, Greenbelt, MD, 32 pp.

Pitts, D. E., J. T. Lee, J. Fein, Y. Sasaki, K. Wagner and R. Johnson, 1977: Mesoscale cloud features observed from Skylab. *Skylab Explores the Earth*, NASA SP-380, eds. V. R. Wilmarth, J. L. Kaltenbach and W. B. Lenoir, NASA Lyndon B. Johnson Space Center, Houston, TX, 479-501.

Revell, C. G., 1983: High resolution satellite imagery of the New Zealand area: a view of mesoscale cloud vortices. *Weather and Climate*, 2, 11-19.

Riehl, H., 1954: *Tropical Meteorology*. McGraw-Hill Book Company, New York, 393 pp.

Svetz, F. J., 1985: Use of space shuttle photography in the study of meteorological phenomena. M. S. Thesis, Naval Postgraduate School, Monterey, CA, 105 pp.

Thomson, R. E., J. F. R. Gower and N. W. Bowker, 1977: Vortex streets in the wake of the Aleutian Islands. *Mon. Wea. Rev.*, 105, 873-884.

Tsuchiya, K., 1969: The clouds in the shape of Karman vortex street in the wake of Cheju Island, Korea. *J. Meteor. Soc. Japan*, 47, 457-465.

von Karman, T., 1911: Uber den Mechanismus des Widerstandes, den ein bewegter Korper in einer Flussigkeit erfahrt. *Goett. Nachr. (Math.-Phys. Kl.)*, 4, 509-517.

Zimmerman, L. I., 1969: Atmospheric wake phenomena near the Canary Islands. *J. Appl. Met.*, 8, 896-907.

INITIAL DISTRIBUTION LIST

		No. Copies
1.	Defense Technical Information Center Cameron Station Alexandria, VA 22304-6145	2
2.	Library, Code 0142 Naval Postgraduate School Monterey, CA 93943-5002	2
3.	Chairman (Code 63Rd) Department of Meteorology Naval Postgraduate School Monterey, CA 93943	1
4.	Chairman (Code 68Tm) Department of Oceanography Naval Postgraduate School Monterey, CA 93943	1
5.	Professor C. H. Wash (Code 63Wx) Department of Meteorology Naval Postgraduate School Monterey, CA 93943	9
6.	Professor P. A. Durkee (Code 63De) Department of Meteorology Naval Postgraduate School Monterey, CA 93943	1
7.	LCDR David R. Markley, Jr. 524 Fairwood Dr. Marysville OH 43040	1
8.	Director Naval Oceanography Division Naval Observatory 34th and Massachusetts Avenue NW Washington, DC 20390	1
9.	Commander Naval Oceanography Command NSTL Station Bay St. Louis, MS 39522	1
10.	Commanding Officer Naval Oceanographic Office NSTL Station Bay St. Louis, MS 39522	1
11.	Commanding Officer Fleet Numerical Oceanography Center Monterey, CA 93943	1
12.	Commanding Officer Naval Ocean Research and Development Activity NSTL Station Bay St. Louis, MS 39522	1
13.	Commanding Officer Naval Environmental Prediction Research Facility Monterey, CA 93943	1

14.	Chairman, Oceanography Department U.S. Naval Academy Annapolis, MD 21402	1
15.	Chief of Naval Research 800 N. Quincy Street Arlington, VA 22217	1
16.	Office of Naval Research (Code 420) Naval Ocean Research and Development Activity 800 N. Quincy Street Arlington, VA 22217	1
17.	Scientific Liason Office Office of Naval Research Scripps Institution of Oceanography La Jolla, CA 92037	1
18.	Commanding Officer Naval Eastern Oceanography Center Naval Air Station Norfolk, VA 23511	1
19.	Mr. and Mrs. David R. Markley 524 Fairwood Dr. Marysville, OH 43040	1
20.	Mr. and Mrs. E. J. Power 179 Crown Dr. Naples, FL 33942	1

17898 2

221097

Thesis
M3435
c.1

Markley
Characteristics of mesoscale island barrier cloud phenomena observed in satellite and space shuttle imagery.

24 AUG 91 37060

221097

Thesis
M3435
c.1

Markley
Characteristics of mesoscale island barrier cloud phenomena observed in satellite and space shuttle imagery.

thesM3435
Characteristics of mesoscale island barr
3 2768 000 75925 2
DUDLEY KNOX LIBRARY